50-kA Capacity, Nitrogen-Cooled, Demountable Current Leads for the SPARC Toroidal Field Model Coil

Vincent Fry, Alexander Zhukovsky, Michael J. Wolf, Philip C. Michael, Rui F. Vieira, William K. Beck, Raheem Barnett, Jose Estrada, Ernest Ihloff, Christopher Vidal, Theodore Golfinopoulos, and Zachary S. Hartwig, *Member, IEEE*

***Abstract*—This paper presents design, fabrication, and operational results for a novel pair of binary Current Leads (CLs). The CLs were purpose built for the SPARC Toroidal Field Model Coil (TFMC) Test Facility at the MIT Plasma Science and Fusion Center (PSFC). The CLs operate stably at current ramp rates up to 50 kA/s and steady-state currents of 50 kA from ambient temperature power supplies to the facility's 20 K test environment. The CLs have three main sections: an upper copper heat exchanger (HEX) cooled with gas nitrogen (GN2) which connects to room temperature power supply (PS); a central liquid nitrogen (LN2) boiling chamber (BC) which vents into the HEX; and a lower Rare Earth Yttrium Barium Copper Oxide (REBCO) Section. The CLs have three distinguishing features: the BCs high surface area maintains $<$1 K temperature difference between their surfaces and the nucleate boiling LN2 within; each REBCO section is composed of six parallel "petals" that were individually qualified prior to installation; indium seals were used to simultaneously provide electrical continuity and hermetic sealing which enabled fabrication without need for braze or electron beam welding qualification processes. Additionally, the CLs can reduce the LN2 boiling pressure and thus temperature which significantly improves the temperature margins within the REBCO Section. The CLs were designed and built within 1.5 years and used successfully to deliver 40.5 kA of current to the SPARC TFMC. Since then they have been thermally cycled over 10 times and operated at both 1 atm and 0.65 atm.**

***Index Terms*—Current lead (CL), high-temperature superconducting (HTS), nitrogen, rare earth yttrium barium copper oxide (REBCO), toroidal field model coil (TFMC).**

Manuscript received 20 September 2023; revised 28 December 2023; accepted 10 January 2024. Date of publication 16 January 2024; date of current version 19 February 2024. This work was supported by Commonwealth Fusion Systems. *(Corresponding author: Vincent Fry.)*

Vincent Fry was with MIT Plasma Science and Fusion Center, Cambridge, MA 02139 USA. He is now with Commonwealth Fusion Systems, Devens, MA 01434 USA (e-mail: vfry@cfs.energy).

Alexander Zhukovsky, Philip C. Michael, Rui F. Vieira, William K. Beck, Jose Estrada, Ernest Ihloff, Christopher Vidal, Theodore Golfinopoulos, and Zachary S. Hartwig are with MIT Plasma Science and Fusion Center, Cambridge, MA 02139 USA (e-mail: zhukovsky@psfc.mit.edu; michael@psfc.mit.edu; vieira@psfc.mit.edu; beck@psfc.mit.edu; jestrada@psfc.mit.edu; eihloff@mit.edu; cvidal@mit.edu; golfit@psfc.mit.edu; hartwig@psfc.mit.edu).

Michael J. Wolf is with the Institute for Technical Physics, Karlsruhe Institute of Technology, 76021 Karlsruhe, Germany (e-mail: michael.wolf@kit.edu).

Raheem Barnett is with Commonwealth Fusion Systems, Devens, MA 01434 USA (e-mail: rbarnett@cfs.energy).

Color versions of one or more figures in this article are available at https://doi.org/10.1109/TASC.2024.3354237.

Digital Object Identifier 10.1109/TASC.2024.3354237

I. Introduction

IN PARALLEL with the development of the SPARC Toroidal Field Model Coil (TFMC) [1], the MIT Plasma Science and Fusion Center (PSFC) designed, built, and commissioned a pair of 50-kA capacity, liquid-nitrogen (LN2) cooled current leads (CLs). These CLs are significantly more powerful than any CLs previously designed and optimized to use LN2 (see Section II-I-A), progressed from conceptual design to 50 kA commissioning in only 1.5 years, and drastically simplify the processes of manufacturing and integrating high-current-capacity CLs into test facilities. These CLs are enabling MIT to test a variety of high-power R&D magnets and will become integral in the design and operation of the SPARC net-energy fusion tokamak being built by Commonwealth Fusion Systems (CFS).

The focus of this article is on the design and operation of the CLs, shown in Fig. 1, designed and built to transmit current from the test facility's room temperature power supplies (PS) to the TFMC. This article is structured as follows: Section II of the manuscript provides an overview of the TFMC, requirements of the test facility, and their implications for the CLs. Section III presents CL background information, the design of the rare earth yttrium barium copper oxide (REBCO) section, and analysis tools. Section IV discusses the "resistive section" made up of the boiling chamber (BC), heat exchanger (HEX), and room temperature terminal. Section V shows the detailed design of the VIPER cold bus cables, the liquid nitrogen (LN2) circuit, and the assembly; Section VI presents an overview of the CL instrumentation. Section VII summarizes representative performance results. Section VIII concludes that the CL performance is well-predicted and met all expectations.

II. TFMC Overview, Test Facility, and Current Leads

A. SPARC Toroidal Field Model Coil

The SPARC TFMC Project was an approximately three-year effort between 2018 and 2021 that developed novel REBCO superconductor technologies [2], [3], [4], [5] and then utilized those technologies to successfully design, build, and test a first-in-class, high-field ($\sim$20 T) representative scale ($\sim$3 m in linear size) superconducting toroidal field coil (see Table I).

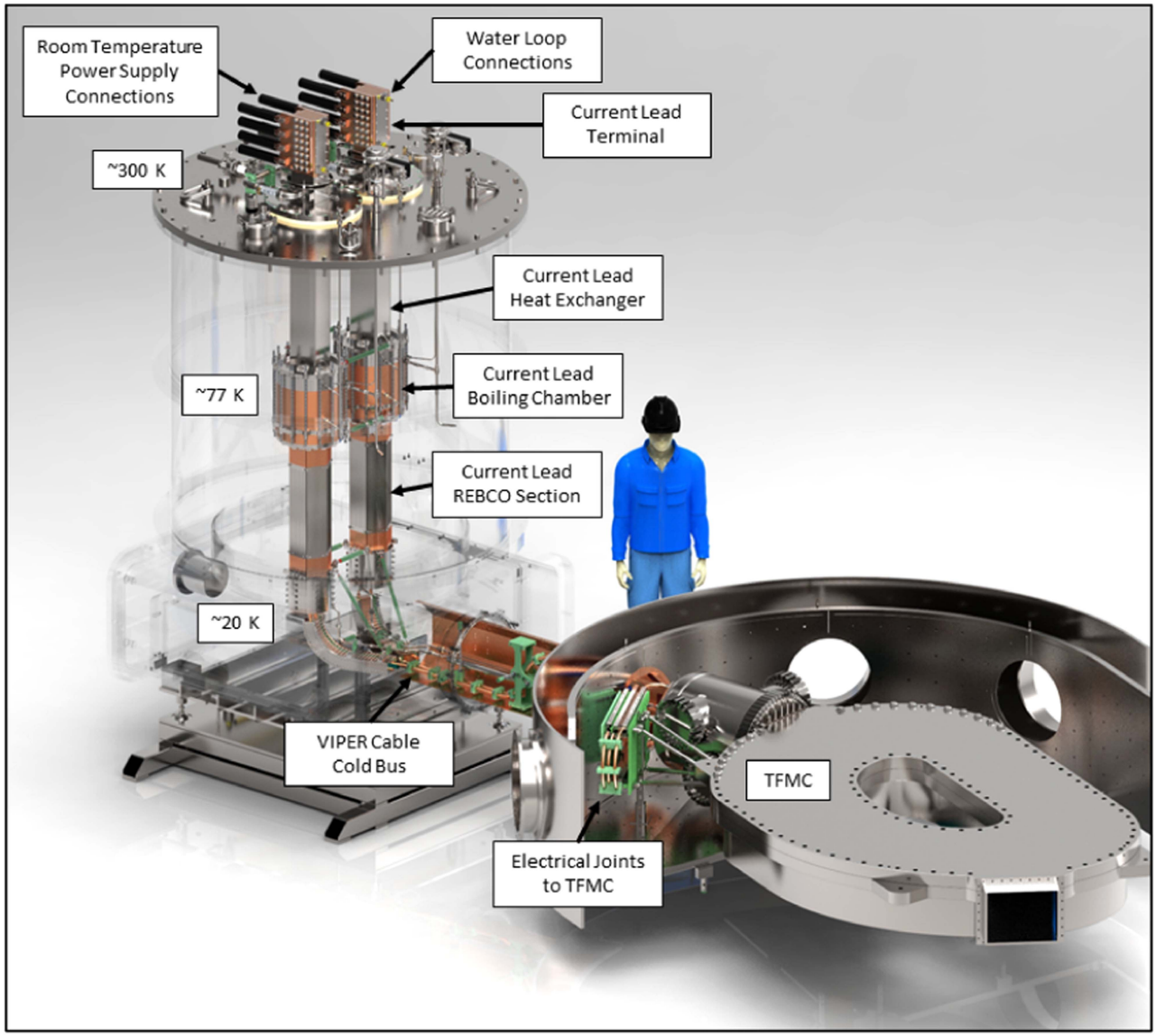

Fig. 1. Rendering of both current leads and their VIPER cold bus connections to the TFMC. The current lead cryostat and internals including the LN2 reservoir and thermal shields are shown as transparent.

With the principle objective of retiring the design, fabrication, and operational risks inherent in large-scale, no-insulation REBCO superconducting magnets for fusion energy devices, the project was executed jointly by the MIT PSFC and CFS as a critical technology enabler of the high-field pathway to fusion energy [6] and, in particular, as a risk retirement program for the TF magnet in the SPARC net-energy fusion tokamak [7]. This article is a part of a collection of papers intended to cover the principal parts of the TFMC Project including the design and fabrication of the magnet [1], [8], the design and assembly of the test facility [9], [10], and an overview of the results [11] from the experimental test campaigns carried out in the fall of 2021.

B. Test Facility Overview

Along with the design and construction of the TFMC, the MIT-PSFC needed to simultaneously stand up a test facility capable of supplying the high currents, high-pressure low-temperature cryogens, and instrumentation and control systems needed to successfully operate the TFMC. An overview of the test facility is presented in [9], whereas the design of the facility's 20 K, 20-bar helium cooling loop is shown in [10].

C. Selection of LN2-Cooled Binary Current Leads

A significant concern during the initial configuration of the facility was the choice of cryogenic coolant for the CLs. The PSFC does not have a significant liquid helium refrigeration (LHe) infrastructure. Among the LHe cooling options considered were: open-loop transfer from a bulk transport container, where consumption could easily exceed 1800 l/day for a pair of conventional, 50 kA-rated, vapor-cooled CLs at idle calculated according to [12], or acquisition of a dedicated, newly commissioned helium cryoplant, neither of which matched the budget or timeline for facility completion.

TABLE I
TFMC DESIGN PARAMETERS

Design Parameter	Value
Overall magnet mass	10 058 kg
Overall magnet size	2.9 m x 1.9 m
Winding pack mass	5113 kg
Winding pack current density	153 A/mm^2
Winding pack inductance	0.14 H
Winding pack amp-turns	10.4 MA-turns
Terminal current	40.5 kA
Number of turns	256
Number of pancakes	16
Total REBCO tape length	270 km
Coolant type	Supercritical helium
Coolant pressure	25 bar (max)
Operating temperature	20 K
Peak magnetic field	20.3 T
Peak Lorentz loading	822 kN/m
Magnetic stored energy	110 MJ

TABLE II
CURRENT LEAD DESIGN CONSTRAINTS

Design Parameter	Value
Lead configuration	Binary lead
Maximum operating current	50 kA
Maximum voltage to ground	10 V
Resistive section	OFHC Copper
Resistive section cooling	Boiling LN2 plus GN2 heat exchange
Nitrogen bath temperature	Variable, down to 68 K as needed
REBCO tape width	4 mm
Minimum temperature margin in REBCO section at atmospheric pressure LN2	1 K
REBCO section operational temperatures	15-80 K
Targeted conduction heat load to 20 K circuit	<25 W/lead

The significant cost and complexity of both of the proposed helium cooling options led to the adoption of LN2-cooled, binary CLs for the facility [13], [14], [15], [16]. The PSFC had significant experience using LN2 for cooling the C-Mod tokamak, and it retains an 18 000-gallon storage tank that could be readily accessed by the test facility CLs [17]. An added complexity for CL testing was that the facility's newly acquired 50-kA PS would not be ready until late in the program. This meant that each REBCO section, with a designed critical current in excess of 50 kA, could not be qualified as a single unit before integration into the test facility.

The CLs were designed to meet the specific needs of the SPARC TFMC, which used a no-insulation, cable-in-plate design [5]. Table II summarizes the design constraints for our binary CLs. The leads featured LN2-cooled copper BCs, gas nitrogen (GN2) cooled copper heat exchangers (HEXs), and REBCO-based lower sections. For the sake of inventory control, the same 4-mm-wide REBCO tape used in the TMFC was also used for CLs' REBCO sections and for the VIPER cold bus from the leads to the TFMC (discussed in Sections III and V-A). The leads were designed to a maximum current of 50 kA (the nominal TFMC current was 40.5 kA) and a maximum voltage to ground of 10 V, which is far above the TFMC's anticipated quench voltage (see [11] for measured voltages during quench). Given the expected voltages during operation and the estimated 1.5-year timeline needed to develop and validate a high-voltage insulation solution, we decided to proceed without Paschen-tight, high-voltage insulation on the CLs.

III. CL BACKGROUND, REBCO SECTION DESIGN, AND ANALYSIS

A. Background

Several pairs of high-capacity CLs, with current ratings above 10 kA, have been designed and built for fusion and other high-field magnet applications. These CLs, for example, [18], [19], [20], [21], and [22], use a "binary" approach, with a resistive (typically copper) upper section and high-temperature superconducting (HTS) lower section to minimize the heat load at the low-temperature end of each CL. The resistive section spans from room temperature to an intermediate temperature, typically between 40 and 80 K, whereas the HTS section extends from the intermediate temperature to the magnet's operating temperature, which is usually below 20 K. A key consideration when choosing between design options is the type and quantity of cryogen needed to operate the CLs. Even with an ideal Carnot cycle refrigerator, the room temperature input power required to remove a 5 K heat load can easily exceed 50 times the heat conducted down the leads [23], [24].

The use of conduction cooling for the resistive sections of CLs is limited to operating currents below 2 kA [25], [26] due to the significant conduction heat loads. To reach higher operating currents, the general tendency is to resort to gas cooling for the resistive lead section. The coolant of choice has generally been helium, given its use in all LTS magnet systems. Helium bath-cooled [27] and supercritical helium (SHe) forced-flow cooling [28], [29], [20], [30], [22] are the most commonly used approaches and have been demonstrated for CLs up to 80 kA. In the last two decades, multiple LN2-cooled CLs [31], [32], [21], [33], [34], [35], [36] have been built with increasing frequency and shown to operate up to 20 kA. Formally, the record 68 kA current for LN2 cooled CLs was demonstrated in [22], where the ITER horizontal CL sample (designed for cooling by 50-K forced flow He gas) was modified for 80-K He cooling and then for LN2 cooling. A part of the HEX was used as a BC for the experiment. The CL was not optimized for LN2 cooling and the decision was made to use 50-K helium for future ITER CL projects.

While the bulk of the heat load from the resistive section is intercepted at intermediate temperature, the lower REBCO section

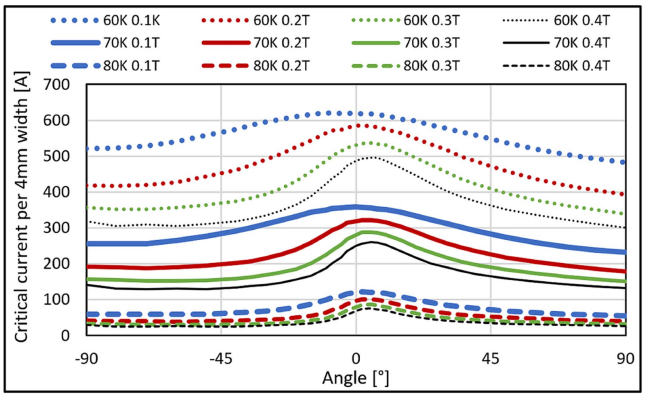

Fig. 2. Critical current data for the CL REBCO tapes as a function of temperature, magnetic field, and field angle.

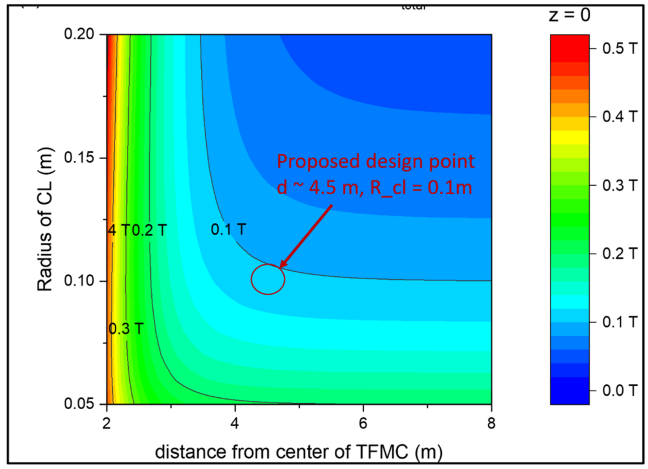

Fig. 3. Magnetic field intensity at the REBCO section as a function of CL radius and distance from TFMC center.

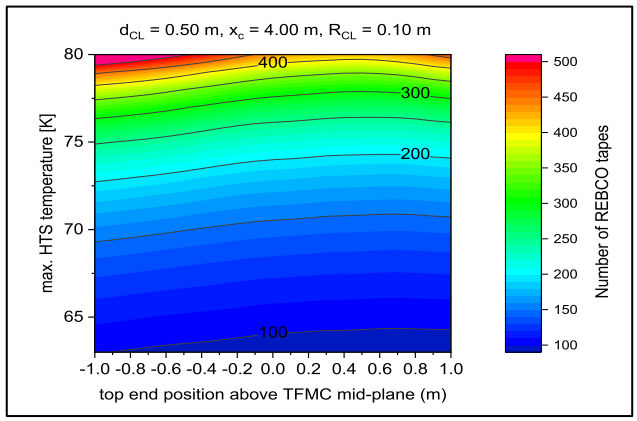

Fig. 4. Required numbers of REBCO tapes in each REBCO section to carry 50 kA as a function of maximum REBCO temperature and vertical position from the TFMC midplane.

is configured to minimize the heat load at its lower temperature end while providing suitable survivability to off-normal events. So long as the REBCO section remains below its current sharing temperature, all current is carried in the superconducting layer and the only heat passed to the cryogenic circuit is generated either in resistive interfaces or thermally conducted along the REBCO section. The REBCO section is typically configured using HTS elements mounted to or embedded in a low-thermal-conducting structural material such as brass or stainless steel to minimize heat load to the cold circuit.

B. REBCO Section Tape Usage

Due to the proximity of the atmospheric boiling temperature of LN2 to the current sharing temperatures of commercially available REBCO tape, the design of the REBCO lead sections is rather tightly constrained, and hence it was analyzed first. The tape for the TFMC facility's CL REBCO sections was provided by CFS. Extensive effort by CFS, both internally and in concert with other laboratories established the field magnitude, field angle, and temperature scaling relations used during the design of the CLs [37], [38]. Fig. 2 shows representative values of critical current versus field angle for the CLs' REBCO tapes, at the temperatures and field amplitudes anticipated near the warm ends of the REBCO lead sections. The results show a substantial drop in performance between 70 and 80 K as well as a significant reduction in performance with a relatively slight increase in magnetic field. The tapes have a Hastelloy substrate that is $\sim$50 μm thick with copper plating $<$10 μm thick on all sides [8].

C. Magnetic Field Calculations

Because of the strong dependencies of the REBCO tape's critical current on both the magnetic field amplitude and field direction, the REBCO sections were designed iteratively, starting with large-scale effects first, with finer scale details added as the design evolved. The dominant magnetic field components imposed on each REBCO lead section are those produced by the TFMC and by the lead section itself. Fig. 3 shows contours of constant, combined magnetic field amplitude from those two contributions, with the distance from the center of the TFMC to the center of the REBCO section plotted on the x-axis, and the nominal radius of the REBCO section plotted on the y-axis.

For this calculation, the TFMC was modeled as a simple magnetic dipole. Because the design operating current for the TFMC was not yet finalized at this stage of the CL design, the dipole strength was set equal to that for the TFMC operating at 50 kA. For the self-field calculation, the REBCO section was modeled using a cylindrical cross section, where the self-field varies as the inverse radius of the lead.

Fig. 3 shows the magnetic field at the top of the REBCO section and the basic design point for the TFMC CLs with a dark red circle. The chosen design point uses a 0.1 m radius for each REBCO lead section, with the leads centered roughly 4.5 m from the center of the TFMC. For this combination, the self-magnetic-field contribution is reasonably small but still dominates the total field at the REBCO sections.

Fig. 4 shows a more refined analysis with the distance from the upper end of the REBCO sections to the TFMC midplane on the x-axis and the temperature at their upper ends on the y-axis. For this analysis the distance between CL centers was set to 0.5 m, the distance from the CLs centers to the TFMC

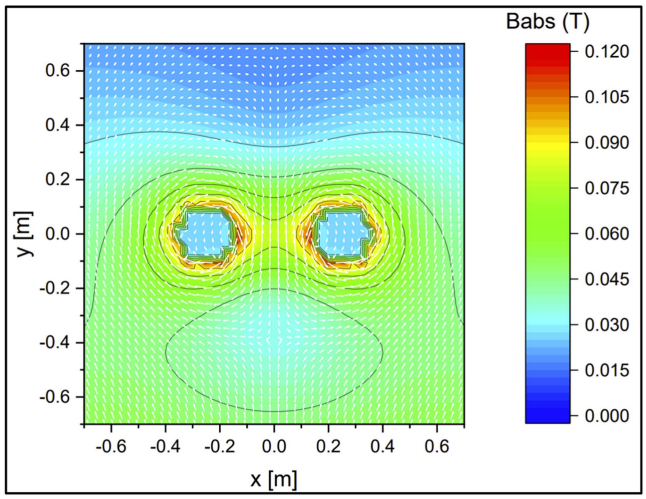

Fig. 5. Magnetic field analysis with 50 kA, hexagonal REBCO sections, 0.5 m distance between CL centers, 4.0 m distance to TFMC center, and 1.1 m height of the upper end of REBCO section relative to TFMC midplane.

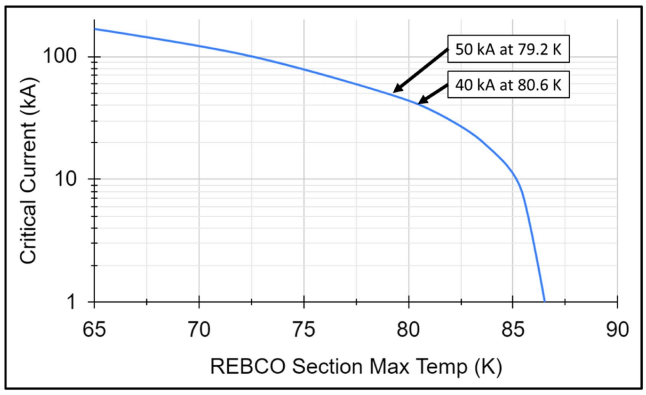

Fig. 6. Critical current as a function of maximum REBCO section temperature.

was set to 4.0 m, and the radius of the REBCO sections was set to 0.1 m. Facility constraints required the top end of the REBCO sections to be above the TFMC midplane and a height of 1.1 m was chosen which corresponded to ∼500 REBCO tapes required to transport 50 kA assuming a maximum temperature of ∼80 K, a 2 K temperature margin above the worst case 78 K expected during operation. The required number of tapes drops rapidly with decreasing temperatures, introducing the possibility of markedly increasing the temperature margin at the upper ends of the REBCO sections with only a modest decrease in temperature. Progressively more refined magnetic field analyses shown in Fig. 5 were then used to: select a hexagonal arrangement of six "petals" for the REBCO sections with 22 stacks of 4 tapes in each "petal" (528 tapes in total), set the 0.95 mm lateral separation between REBCO tape stacks in each petal, and set the current polarity direction for each CL relative to the TFMC's magnetic field. This hexagonal arrangement minimizes perpendicular field components on the tapes while keeping the geometry manufacturable.

Fig. 6 shows how the predicted critical current of this final arrangement decreases with increasing temperature.

D. Cold End Heat Load and Quench Management

The required amount of stabilizer in the REBCO sections is principally determined by the peak temperature allowed during off-normal events. In addition to the thin copper stabilizer layer plated onto each REBCO tape, typically, brass, stainless steel, or other alloys are added to the structure to enhance their response to off-normal events. Alloy stabilizers are generally used due to their rather low thermal conductivities and relatively flat electrical resistance versus temperature. Low thermal conductivity limits the heat load to the cold end of the lead, whereas flat electrical resistivity minimizes the chance for abrupt thermal run-away, as the heat capacities of these material increase much more rapidly with temperature than does their increase in electrical resistivities.

Because it has significantly higher yield stress than brass, we selected stainless steel 304L for the REBCO section stabilizer to provide the mechanical strength needed to withstand stresses from multiple processing steps during petal fabrication. The adoption of peak temperature below 150 K following a minimum 5 s discharge time during either quench or loss of cooling at 50 kA resulted in the adoption of a stainless steel cross-sectional area of roughly 476 mm^2 for each petal and a calculated conduction heat load of roughly 5 W per CL to the 20 K end.

Loss of cooling analyses showed two key results that gave confidence in the CL operation without needing experimental validation that could have jeopardized the facility. First, during nominal operation with ∼100 mm of LN2 within the BC, each CL has ∼7.5 kg of LN2 volume stored within it. In the event of loss of LN2 supply to the CLs, each CL could continue to operate at 50 kA for ∼15 min before running out of LN2. Second, once out of LN2 the thermal inertia of the CL and REBCO section is such that thermal quench takes nearly 3 more minutes to occur at 50 kA transport current.

E. Analysis

A combination of 1-D and 3-D analysis codes was used to optimize the design as well as to compare its measured performance to design expectations.

1-D analysis of CLs has been refined over the years [39], [40], [41] and the code CURLEAD was instrumental in the initial thermal optimization of the design. Before production, an in-house 1-D MATLAB (MathWorks Inc., 2021b) code was created and verified against the CURLEAD results. Both codes divided the CL into many subsections, each with a material property set, length, area, and any relevant additional heating inputs or outputs. GN2 heat exchange could be directly calculated using known equations for laminar flow through the rectangular channels in the HEXs (see Fig. 11). A Nusselt number of 7.54 was used which corresponds to a low Reynolds number laminar flow through parallel plates at a constant temperature. These models were not detailed enough to query specific locations of voltage taps or thermocouples, and there were concerns that the geometry of the boiling chamber could not be accurately represented and thus would lead to anomalous predictions. This led to the development of a secondary 3-D model built within

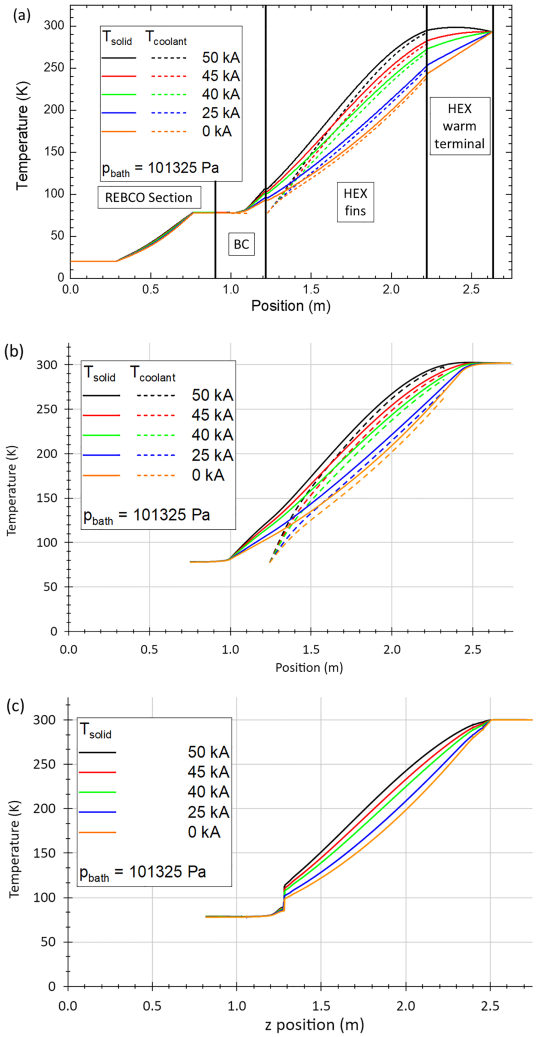

Fig. 7. Temperature versus position of the solid and/or coolant of the CLs at various operating currents as predicted by (a) early 1-D CURLEAD analysis with the topmost point pinned at 30 C, (b) near-final MATLAB 1-D analysis meant to mimic CURLEAD and introduce 30 C water heat exchange along the entire face of the upper terminal, and (c) final 3-D COMSOL analysis will detailed CL geometry that uses gas nitrogen heat removal from the 1-D MATLAB model to simplify the simulation. Note that the COMSOL output is the true z position in the geometry.

COMSOL Multiphysics version 5.3. There were two primary goals of the 3-D model: first, to study the effect of the assumed LN2 boiling heat transfer characteristics on the temperature distribution within the BC and REBCO sections; and second, to extract simulated data from the precise locations of known instrumentation to correlate between simulation and measurement. The range of assumed LN2 boiling heat transfer characteristics was bounded by previously published correlations found in [42], [43], [44], [45]. The final released geometry was input directly into COMSOL from the HEX to the upper copper pieces of the REBCO section. Current, its associated interfacial heating, and the assumed LN2 boiling heat transfer equations within the BC were applied to their corresponding faces in the model. Solving the full GN2 flow equations within the HEX overcomplicated the model so instead the outputs from the 1-D MATLAB code were used to subtract the relevant amount of heat from the HEX

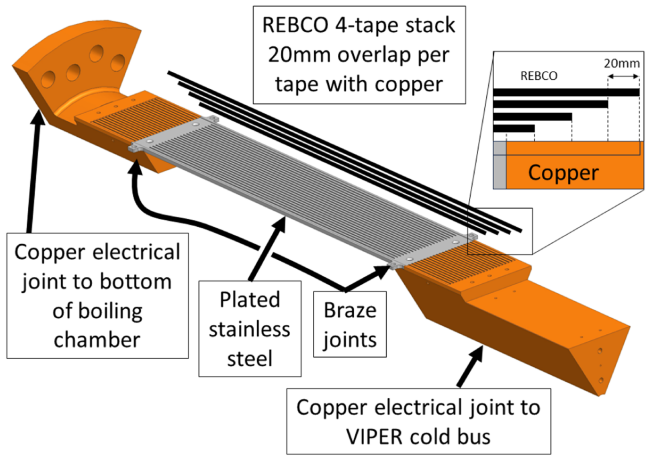

Fig. 8. Solid model image showing one of the brazed "petals" of the REBCO section before REBCO soldering operations. Also shown on the stainless steel plate are four small tabs used only for plating, these are removed before REBCO soldering.

and this method proved very accurate (see Section VII). Using this model, LN2 boiling heat transfer equations could be altered until the simulated temperature ranges within the BC matched those that were measured (see Fig. 21).

Fig. 7 shows the outputs of temperature versus position for the three analysis methods used. Note that both CURLEAD and MATLAB outputs are 1-D approximations of the CL geometries, so their length scales do not exactly match the true z-position output from COMSOL. This also explains the apparent jump in temperatures of Fig. 7(c) at position ~1.3 m which is the lid of the BC as it increases radially in temperature between the BC walls and the HEX connection. All three models showed good agreement with the 1-D models accurately predicting nitrogen gas output temperatures (see Fig. 22) and the 3-D model accurately outputting temperatures in the BC and the HTS section warm end (see Figs. 20 and 21).

Further 3-D models were generated for all electrical joints containing REBCO within the CL assembly. These were used to predict a range of expected operating resistance for input into the CL thermal models.

F. Manufacturing and Test Considerations

Because the 50 kA current source procured for the TFMC test facility would not be completed in time to test subsystem components, testing of the CL REBCO petals was limited to an existing, in-house 16 kA supply. For both this reason and ease of manufacture, the REBCO section was subdivided into six "petals," which are placed in parallel to provide the full current carrying capacity for each CL. The use of REBCO as opposed to other conductors such as Bi2223 was motivated by: our extensive experience making soldered REBCO joints, our desire to not have multiple conductor technologies, and all analyses showed the REBCO would remain thermally stable with our anticipated resistive and conductive heat loads.

Fig. 8 shows a solid model image for one of the petals before REBCO insertion. The body of the petal is composed

TABLE III
MEASURED AND SIMULATED ELECTRICAL RESISTANCES

Tap pair description	Tap pair designation	Measured resistance at 40.5 kA [nOhm]	Simulated resistance at 40.5 kA [nOhm]
Overall HEX slit cut region	V_OVRALL	726.8 +/– 5.7	728.8
Upper ~1/3 of HEX slit cut region	V_HI	334 +/– 15.2	322.7
Middle ~1/3 of HEX slit cut region	V_MID	247.6 +/– 7.5	244.0
HEX to BC Lid, with indium interface	V_HBC	43.7 +/– 2.9	51.6
BC Lid to BC Base, with indium interface	V_BC1	51.5 +/– 0.1	53.1
BC Base to upper ends of HTS section, with indium interface	V_BC2	9.2 +/– 2.9	10.2
Copper to REBCO soldered joints at top and bottom of HTS section	V_HTS,ave	4.0 +/– 0.2	5.0
Copper to REBCO soldered joint at bottom of HTS section	V_HTSL	0.1 +/– 0.1	0.8
Copper at bottom of HTS section to VIPER cable jumper	V_TRM,ave	1.1 +/– 0.1	1.5

of a 530-mm long, 114-mm wide, 4.8-mm thick sulfamate-nickel-plated stainless steel plate brazed at either end to two, large OFHC copper end pieces. The upper end piece (toward the left) is flanged to facilitate connection to the underside of the BC, whereas the lower end has a cylindrical inner surface to facilitate clamping around a 21-mm diameter VIPER cable [2], which serves as the CL's 20-K current connection. Unlike standard VIPER cables, these used a solid core to increase their conduction cross-section, being cooled only at their connection with the facility cold bus, which is actively cooled as part of the facility's supercritical helium circuit [10].

Following inspection and clean-up from the braze operation, 22 stacks, each containing 4 REBCO tapes were soldered into slots machined into the outward-facing surface of each petal. The slots extend 80 mm into each of the copper end pieces and include a stair-stepped arrangement of the tape stack ends that brings the REBCO-coated-conductor-side of each tape into direct contact with the copper end piece, facilitating direct current transfer into each tape in the pedal. Each tape has ~80 mm^2 of soldered contact with the copper on either end.

In preparation for soldering, fluxed tape stacks and thin solder foils were placed in the grooves. The ability to work on flat, horizontal plates greatly simplified the setup for soldering. The entire assembly was installed in a vacuum bag, to firmly press the tapes into their slots, and placed into an air furnace to flow the solder. Resistive heaters and thermocouples were installed at select locations along the assembly to ensure a more uniform temperature distribution. Smaller scale prototypes were used before routine production to confirm braze bond quality, solder processes, and electrically test the tapes, which showed no measurable degradation from start to finish. Three full-scale petals were electrically tested in LN2, demonstrating critical currents from 9.1 to 10.5 kA and index numbers (n) greater than 25, depending on the current ramp rate. The results were very close to the predicted critical current of 9.9 kA. Analysis of the six assembled petals during operation with atmospheric-boiling LN2, magnetic self-field, and TFMC stray field resulted in the plot in Fig. 6. Measured resistances are shown in Table III and were low enough to have a negligible impact on HTS temperatures.

Fig. 9 shows the arrangement of an assembled REBCO section. The upper surface of the REBCO section is bolted to

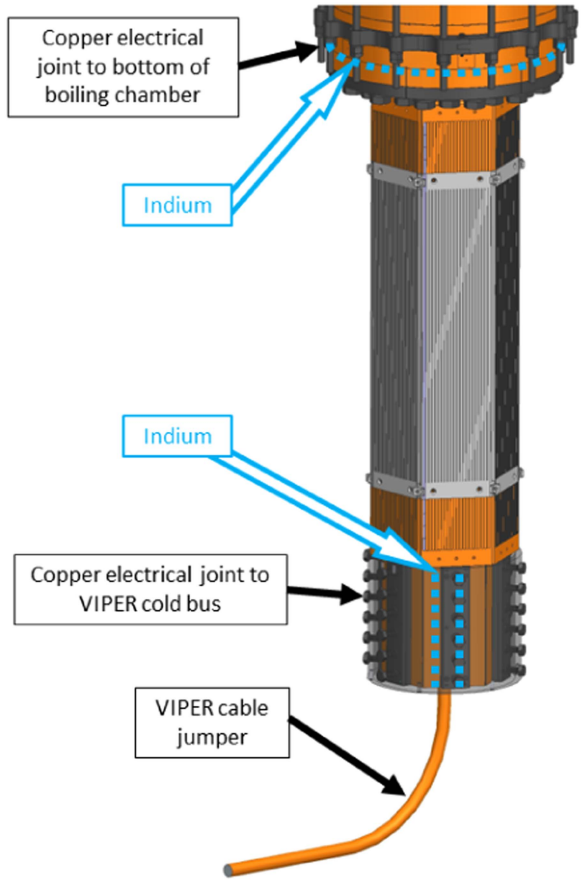

Fig. 9. Solid model image showing a fully assembled REBCO section with the thick stainless steel clamping tube around the VIPER cable shown as transparent.

the BC using indium wire as a compliant electrical interface. The arrangement used a split stainless steel ring inserted into a radial groove in the BC, stainless steel spreader plates pressed against the underside of the copper flanges, and M20 bolts with Belleville washers to generate a nominal clamping pressure of roughly 30 MPa. The lower ends of the petals come together as a cylindrical interface, similar to a machine tool collet. The inner surface of this collet was compressed onto the outer diameter of the VIPER cable, also using indium wire as a compliant electrical interface. In this case, stainless steel

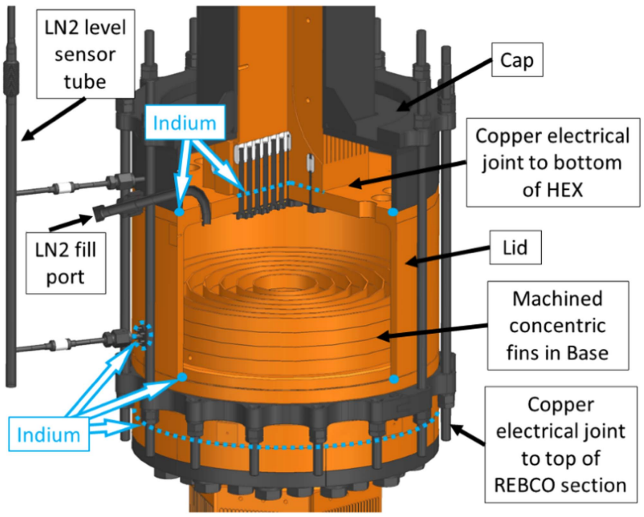

Fig. 10. Cutaway solid model image showing a section view of the BCs. The concentric fins in the BC base can be seen as well as the slit-saw grooves in the HEX and the bolted indium joint configurations.

spreader plates and Belleville washer stacks were mounted to the exterior surfaces of the copper petals. A thick-walled stainless steel tube with M10 bolts installed in threaded holes was used to apply radially inward clamping pressure to the VIPER cable.

Thermal analysis of the as-built configuration of six petals reveals that the conductive heat leak to the 20-K test article is less than 5 W per CL.

IV. Resistive Section

The features described in this section are all located above the REBCO section of the CL. All current is transported through large copper pieces with no REBCO present.

A. Liquid Nitrogen Boiling Chamber

The LN2-cooled BC for each CL provides an intermediate temperature station between the ∼300 K environments at the PS connection and the TFMC's 20 K test environment. Approximately half of the total heat generated by the CL is absorbed in the BC by boiling LN2. The BC also serves to maintain a stable temperature at the top of the REBCO section with its large surface area and thermal mass, as well as high heat of vaporization of LN2. To limit the temperature difference between the saturation boiling temperature of the LN2 coolant and the temperature at the upper ends of the REBCO sections, the wetted surfaces of the BC are designed with sufficient surface area to maintain nucleate boiling conditions throughout their intended operating range. For our design, this was achieved by machining a series of concentric fins into the BC base as shown in Fig. 10.

The section view in Fig. 10 shows that each BC is composed of three major components: an OFHC copper base, containing the circular fins mentioned above; an OFHC copper lid, which connects the base to the neighboring gas heat exchanger (HEX) section; and a stainless steel cap, which separates the boil-off GN2 from the surrounding cryostat vacuum.

Atmospheric boiling heat transfer coefficients for LN2 for a variety of geometries can be found in [42], [43], and [44], whereas reduced-pressure measurements are much harder to come by as presented in [45]. At atmospheric conditions, heat transfer per the Kutateladze correlation provides a relatively conservative heat flux estimate of 3500 W/m^2, whereas at 0.2 atm, this drops to approximately 1500 W/m^2. For conservatism, the BCs were designed to maintain less than 2 K wall-to-liquid temperature differential while operating at 0.2 atm. This resulted in less than 1 K temperature differential during atmospheric pressure operation [see Fig. 21(b)]. Initial 1-D CL simulations showed roughly 1270 W heat transfer to the LN2 at 45 kA so the BC base with cooling fins and BC walls was designed to provide at least 0.85 m^2 total heat transfer area.

The BC base was machined from a single piece of 15-in diameter OFHC copper, with seven concentric vertical fins machined into it to provide the desired heat transfer area. Each 70-mm-tall fin has steps reducing its thickness toward the top, which are intended to interrupt bubble formation that would otherwise prevent fresh LN2 from reaching the surfaces. Two radially directed holes near the base of the fins allow for equalization of the LN2 level. The nominal height of LN2 within the BC can be controlled from 0 to 150 mm above the base of the fins, and the nominal range was 80–120 mm during operation.

The LN2 level in each BC is monitored using an American Magnetics Inc. Model 1700 capacitive level sensor. The level sensor is installed in a small tube, offset from, but connected near the base and upper edge of the BC through ceramic insulators procured from CeramTec. LN2 for the BCs is provided from a common LN2 Reservoir (described in Section V-B); it passes through a pair of proportionally controlled, pneumatically operated WEKA DN6 valves to maintain the targeted level in each BC.

To ensure adequate temperature margin at the upper ends of the REBCO sections, the nitrogen circuit was designed to operate at reduced pressure if the need to reduce BC temperatures ever arose. Our design calculations indicated that the maximum anticipated flow through our leads could be accommodated by one Atlas Copco DZS 100 VSD+ claw pump for each CL. These pumps provide sufficient capacity to reach 300 mbar in each BC, corresponding to a boiling temperature of roughly 68 K.

The BC lid and stainless steel cap in Fig. 10 are firmly compressed against the BC base, with indium wire seals at each interface, using a set of M12 threaded rods. These rods connect at the top to a ring that presses down on the cap and connects at the bottom to the same split clamp that connects the REBCO section to the BC. More details on indium sealing are presented in Section IV-D.

The BC lid and neighboring HEX are similarly electrically connected with a compressed indium joint by installing bolts through the underside of the Lid and into threaded stainless inserts at the bottom of the HEX. The boil-off GN2 needed to cool the HEX passes through a series of holes in the BC lid near its outer diameter.

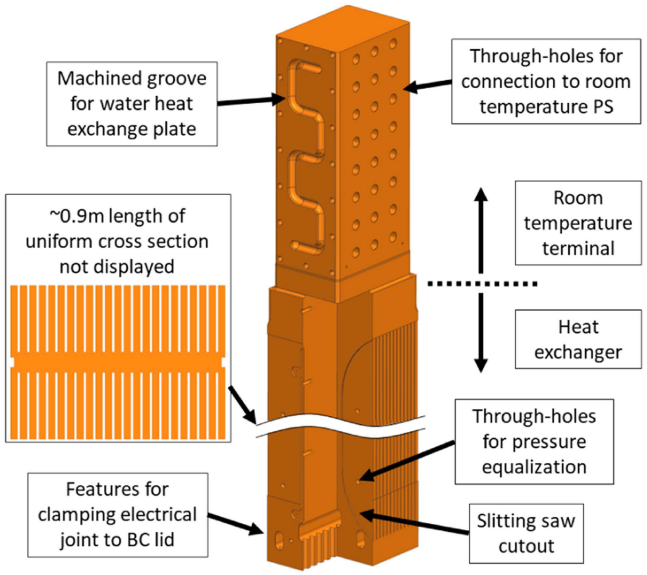

Fig. 11. Cutaway solid model image showing the entire HEX, which is one monolithic machined piece of OFHC copper with the room temperature terminal occupying the top ~0.5 m and heat exchanger at the bottom ~1 m.

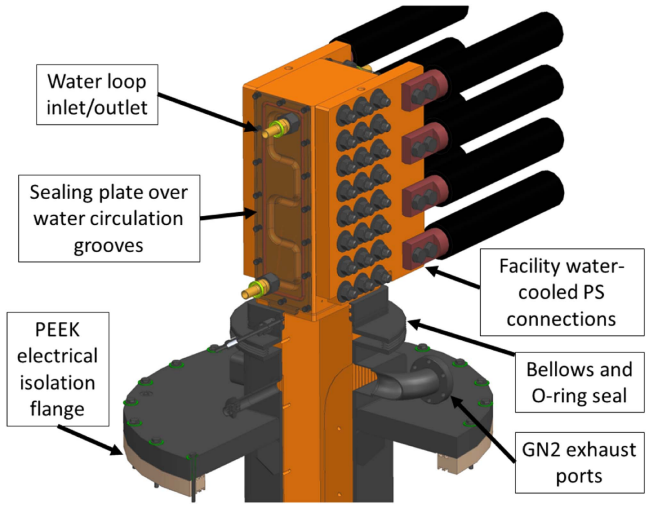

Fig. 12. Cutaway solid model image showing the room temperature terminal of the HEX with integrally machined grooves for distilled water flow. The stainless steel cover plate is shown as transparent.

B. Gaseous Nitrogen Heat Exchanger

The heat exchanger feature described here is the lower ~1 m section of a single ~1.5 m long monolithic piece of machined OFHC copper referred to as the HEX and shown in Fig. 11.

The CL HEXs are designed to transmit current to the BCs while limiting thermal conduction. The HEX cooling grooves must also have both sufficient wetted perimeter and cross-sectional area for low-pressure-drop heat exchange with the GN2 passing through it. A widely cited optimal shape factor for gas-cooled CLs with a 77-K intercept, relating their design current I, cross-sectional area A, and lead length L is defined as an $I{\cdot}L/A$ ratio of 5e6 A/m. [24]. To be conservative to resistive heating our goal was to be below this when operating the TFMC at ~40.5 kA, with a final value of 4.1e6 A/m. This suggests that the optimal current with zero heat load into or out of the room temperature terminal is ~50 kA, which is in agreement with the 1-D analysis in Fig. 7(b).

Manufacturing was a large concern, and the short timeline required the use of known processes and minimal development time. The NHFML "jelly roll" [35] and ASIPP "foil-pressed" [31] approaches were both considered but unknowns surrounding solder and braze development were deemed too risky. Similarly, the room temperature terminal is typically brazed to the HEX, but we chose instead to combine them both into one monolithic piece of 175 mm wide, 125 mm thick, and 1.5 m tall copper bar to simplify this critical interface. The final design used 2-mm slitting saws to cut parallel sets of ~1 m long grooves 50.8 mm deep into two opposing faces of the copper. Figs. 10–12 show cutaway views revealing these grooves in the HEX. This method produced a high enough wetted perimeter and cross-sectional area for nitrogen flow without the need for any brazing operations. The large diameter of the slitting saws naturally provides a curved entrance and exit for the nitrogen flow. Holes are periodically drilled perpendicularly through the fins to equalize mass flow, and the entire structure is later made vacuum-tight by welding four stainless steel plates together with a tight fit around the HEX shown in Fig. 12.

The resulting slow, laminar flow through these grooves has a low-pressure drop and low Nusselt number. A combination of CURLEAD and custom 1-D MATLAB steady-state codes was used to simulate copper and nitrogen properties and a length of ~1 m was found to be sufficient to warm the nitrogen gas close to room temperature by the time it exited while operating at 45 kA current.

C. Room Temperature Current Terminal

The remaining ~0.5 m of the length of stock in the HEX was machined into features that interface with the PS bus and must have temperature regulation to prevent condensation or icing that could potentially cause a loss of vacuum and/or loss of voltage standoff. This is also shown in Fig. 12.

Design recommendations from the ITER CLs for contact area with the PS were followed which include: current density ~2 to 3 A/mm^2 to prevent excessive heating and bus surface contact <0.5 A/mm^2 [18]. The final values at 40.5 kA were 2.5 A/mm^2 and 0.5 A/mm^2, respectively.

Early 1-D analysis of the CLs showed ~1.2 kW heating required at zero current to maintain 30 °C at the room temperature terminal of each CL. A 3.5-kW heater/chiller water circulation unit was installed which can provide temperature-controlled water circulation up to 30 °C for both CLs and eliminates the need for separate resistive heaters. To further simplify the design, a groove for the coolant was cut directly into both sides of the terminal as shown in Figs. 11 and 12. A simple O-ring-sealed plate was placed over top, and a flexible rubber tubing was used to route the distilled water flow to the heater/chiller. The stainless steel shell surrounding the HEX is hermetically sealed to the copper by a double O-ring seal around the base of the room temperature terminal, which has large flexible edge-welded

bellows to allow for differential thermal contraction between the HEX and surrounding stainless steel shell during cooldown.

D. Indium Joints and Vacuum Seals

Due to the significant schedule challenges facing the TFMC Project, the team was wary of adopting brazing and electron beam welding as the primary means for connecting subcomponents. These processes tend to be nonreversible and if done incorrectly result in costly procurement of replacement parts and/or lengthy schedule impacts to re-machine components. There are also relatively few vendors with these capabilities particularly at the ∼3 m sizes necessary and there tend to be lengthy vendor qualification and process development timelines. Combining subcomponents into monolithic parts wherever possible and using indium seals between components provided a significant reduction in schedule and technical risk.

To support this design choice, the team relied on internal knowledge of indium sealing techniques and performed an extensive literature review. Internal knowledge at the MIT PSFC dates back over 25 years in the use of indium for a variety of applications, and many of the same people are still working at the PSFC and could contribute to this project. A large indium seal for liquid helium was designed in the Pulse Test Facility [46] at the MIT PSFC and many electrical interfaces for REBCO-cable joints [47], [48], [49] were built to support the TFMC and various VIPER cable designs. Literature review revealed a variety of articles on indium seals [50], [51], [52], [53], [54], which demonstrated seals of reasonable size sealing up to 177 bar of helium at 77 K.

Six different indium interfaces were successfully implemented on each CL and are shown in Figs. 9 and 10: an electrical connection between each HEX and BC's copper lid; a vacuum-tight connection for the lower level sensor side port; a vacuum-tight connection between the BC lid and its stainless steel cap; a vacuum-tight and electrical connection between BC lid and BC base; an electrical connection between BC base and REBCO section; and an electrical connection between REBCO section and VIPER jumper. To preserve the vacuum integrity in the CL and TFMC test cryostats, which share a common vacuum, it was essential that all CL nitrogen remain within the CL boundaries. All of these seals were implemented on a prototype "Mini Boiling Chamber" that used representative materials and interfaces at roughly half scale. The sample was dunked in LN2 over five times and was helium leak-tight at an internal pressure of 2 bar. All seals performed successfully as long as surfaces were kept clean and scratch-free, and there was constant elastic compression on the seals. All indium seal surfaces were carefully protected, cleaned, and silver plated before assembly.

V. VIPER Cold Bus, Nitrogen Control, and Assembly

A. VIPER Cable Cold Bus

A series connection of three different VIPER cables sits between each CL and its respective terminal on the TFMC. The first is a short VIPER "jumper" cable, which is connected at the bottom of the CL REBCO section and is not actively cooled. This VIPER jumper connects to a second VIPER "cold bus," which travels most of the ∼3 m distance toward the TFMC and is actively helium-cooled. The third VIPER "shunt" connects on one side to the cold bus, on the other to one of the TFMC terminals, and is not actively cooled. The jumpers and cold bus are shown in Fig. 13.

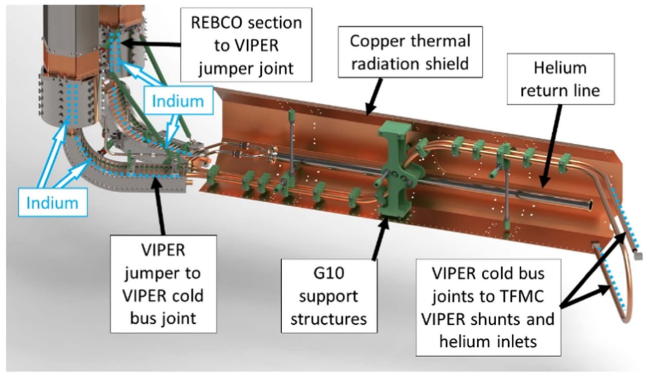

Fig. 13. Cutaway solid model image of the viper jumpers, cold bus, and associated structural G10 clamps. Not shown are the TFMC VIPER shunts on the right-hand side, which can be found in more detail in [8].

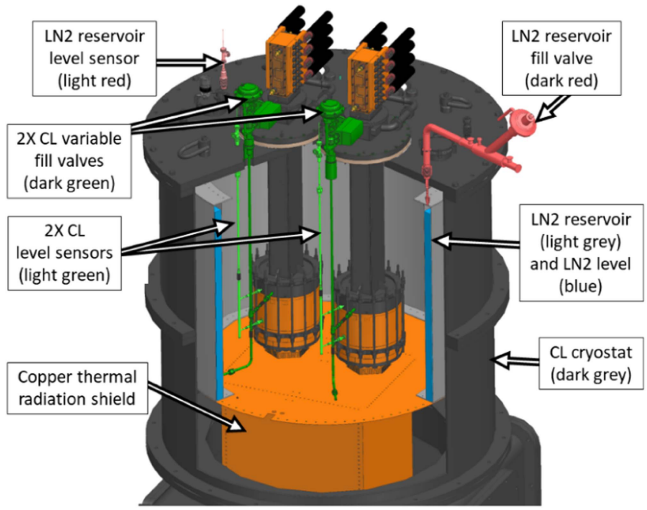

Fig. 14. Cutaway solid model image with false coloring showing a cross section of the CL cryostat and LN2 reservoir to reveal internal features: LN2 reservoir (light gray), LN2 reservoir fill valve (dark red) in the top right, LN2 level sensor (light red) in the top left, two CL fill valves (dark green), two CL level sensors (light green), and copper thermal radiation shield.

The VIPER jumper was connected to the CL before integration into its cryostat (see Fig. 15), at which point the VIPER cold bus was installed from the TFMC side through the vacuum tunnel toward the CL cryostat. The VIPER shunts were integrated into the TFMC [8] and then lowered with the coil into the main cryostat before being connected to the VIPER cold bus.

A small amount of exhaust helium from the TFMC at ∼22 K is sent parallel down the central coolant hole of both VIPER cold bus cables where they make an electrical joint to the shunts and exits at the end of the electrical joint with the jumper cables at the base of the CLs. The cold bus has a significant operational margin due to its low temperature and low field: a

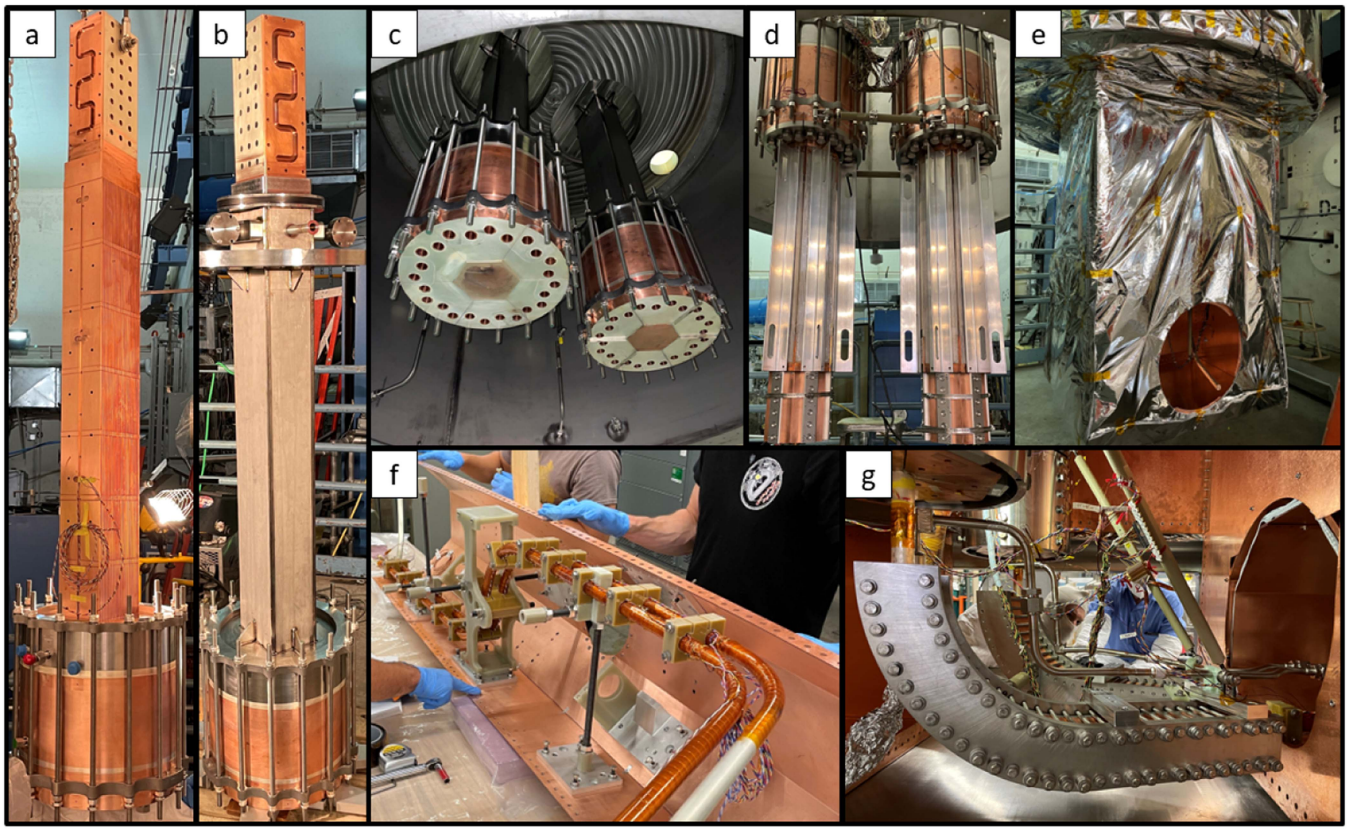

Fig. 15. Photos from various stages of building the CL assembly. (a) Completion of indium seals on the resistive section. (b) Completion of welding the shell and vacuum-tight acceptance. (c) Installation of both resistive sections and LN2 reservoir in the cryostat lid. (d) Installation of both REBCO sections, also shown are braces used only for installation that are later removed. (e) Completion of VIPER jumpers, copper thermal shield, and MLI wrap. (f) Build process for the VIPER cold bus and structural supports. (g) VIPER jumper to VIPER cold bus joints under the CL.

critical temperature at 45 kA of ∼60 K and a critical current at 25 K of ∼100 kA. Routing the cables in close proximity to each other enables the repulsive IxB electromagnetic forces to be supported by clamping the two cables together. Fig. 13 shows both cables and a series of G10 clamps that transmit net body loads to the surrounding radiation shield. More clamps, not shown in Fig. 13, transmit structural loads from the thermal shield onto the cryostat walls. A large sweeping bend in the cable bus accommodates the thermal contraction that occurs while keeping the tensile strain on the REBCO stacks very conservative at <0.1%.

B. LN2 Reservoir and Controls

Due to the novel nature of the CL design, it was decided that each CL should have independent LN2 supply control which provided safety if their performance was not equal (see Sections VI and VII where it is shown that they did perform identically). This decision led to the design shown in Fig. 14 with an annular LN2 reservoir located around the CLs that receives LN2 from the facility and then LN2 supply into each CL is controlled independently with flow-control valves.

This design provides a variety of benefits: independent and simple bi-linear feedback loop control on both CLs; the LN2 reservoir has its own internal level control allowing for control of the inlet pressure to the flow-control valves of each CL; the LN2 reservoir shields the resistive portions of the CLs from thermal radiation from the cryostat sidewalls; and the bottom of the LN2 reservoir allows simple mounting of a conductively cooled copper thermal radiation shield to surround the REBCO sections.

Fig. 14 shows a cross section of the CL cryostat and the LN2 reservoir.

C. Assembly and Qualification

During electrical testing of the REBCO section petals, defects were noticed in some of the REBCO stacks that ranged from small depressions to short delaminated lengths. All petals were thermally cycled in LN2, and a total of 34 defects were found across 9 petals. Assuming in the worst case that all defects were fully destructive of the underlying REBCO stacks, there was sufficient critical current margin in the nondamaged stacks to achieve at least 45 kA, well above the target operating current for the TFMC. Assembly continued, the TFMC was successfully tested, and the CLs have since been operated at currents up to 50 kA with no observed degradation in superconducting performance.

The CLs were constructed by first connecting the bottom of the HEX to the top of the BC lid using a compressed electrical indium joint. The stainless steel cap of the BC lid was then

placed over top, and indium wires were put into the two key-and-groove seals. The BC lid had its capacitive level sensor bulkhead indium seal tightened and then was placed over the BC base with two more indium wires making electrical and vacuum connections. Split clamp plates were then inserted into the BC base, a clamping ring was put over the stainless steel cap, and threaded rods were tightened to compress both indium seals. Every indium connection was allowed to creep for 24 h before retorquing. At this point, the indium seals were qualified by filling the BC with LN2 five times to thermally shock the system, then a large cover was placed over the HEX with O-rings that sealed to the stainless steel cap to allow evacuation and helium leak checking of all the seals. Both CLs finished qualification with no detectable leaks. One finished CL at this point in the process is shown in Fig. 15(a), and further assembly stage photos are also shown. Experience with these types of indium seals has demonstrated they are fully reversible and can be re-assembled multiple times when proper care is taken. The CLs have since been thermally cycled nearly ten times with no leaks.

The four flat stainless steel walls around the HEX [shown in Figs. 10, 12, and 15(b)] were then welded to each other and to the stainless steel cap along with the large upper flange, bellows, double O-ring seal, and exhaust ports. The entire resistive section was then helium leak checked. Both CLs passed successfully.

A large assembly frame was constructed and the CL cryostat lid was placed on top. The LN2 reservoir was brought in from below and lifted up so it hung from the cryostat lid. The resistive sections of both CLs were installed into the CL cryostat lid [see Fig. 15(c)] on top of PEEK flanges for electrical insulation. The REBCO sections were bolted to the bottoms of the BCs [see Fig. 15(d)] and the VIPER jumper cable joints were made. Instrumentation was completed with wires passing through hermetic feedthroughs installed in the lid of the cryostat. Finally, the copper thermal radiation shield was bolted to the underside of the LN2 reservoir that surrounds the REBCO section. The copper shields are removable for access and use Apiezon N grease to increase the thermal contact between them. Both the reservoir and copper shields were covered with 25-layer MLI blankets to further reduce radiative heating [see Fig. 15(e)]. The entire assembly was placed into its cryostat before final leak checks and was then moved into the final position and coupled to the TFMC cryostat.

VI. Instrumentation

Figs. 16 and 17 show illustrations of the instrumentation used to monitor and control the operation of the CLs. Because both leads were instrumented identically and because they showed near identical operating characteristics, only one lead is shown. The signal names used by the facility HMI control system are outlined with black rectangles. Because we do not distinguish between them in the discussion of results, the lead designations, LDN for the negative polarity CL and LDP for the positive polarity CL, have been removed to simplify the signal names. To highlight the instrumentation arrangement, the CL cryostat vacuum shell and conduction-cooled portions of its thermal shield have been similarly suppressed.

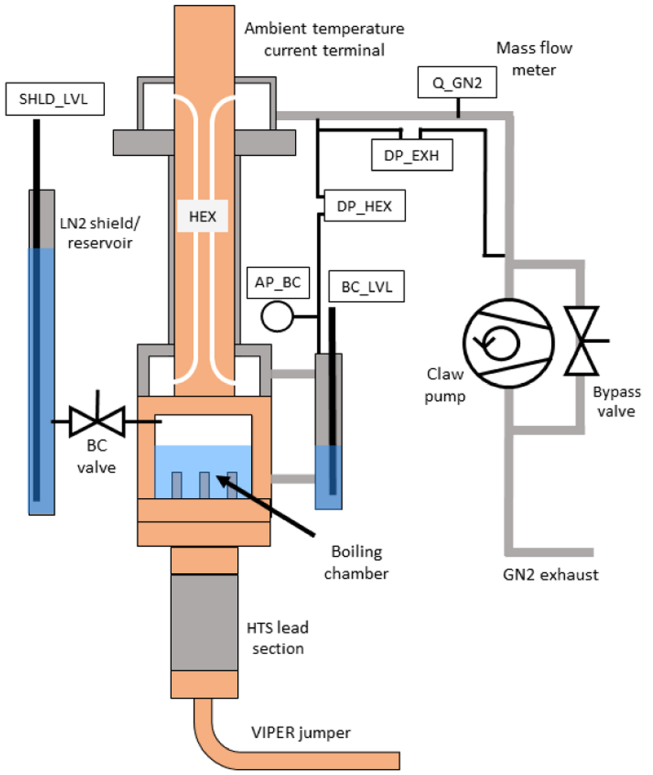

Fig. 16. Instrumentation used to monitor and control the flow of nitrogen into and out of the CLs.

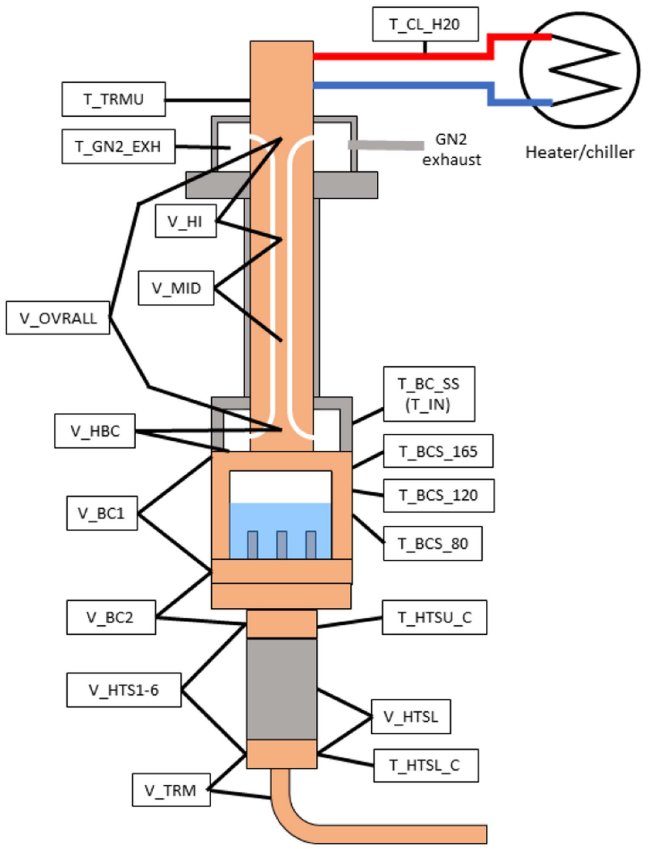

Fig. 17. Voltage tap and temperature sensor arrangement used to characterize the performance of the CL.

Fig. 16 shows the arrangement of the scheme used to monitor and control the flow of nitrogen into and out of the CLs. A partial section view of the cryostat's LN2 reservoir is shown on the left-hand side of the figure. The height of LN2 in this reservoir is monitored by the SHLD_LVL signal, whose controller automatically maintains the LN2 level between low and high set-point limits. The height of LN2 in each BC, BC_LVL, is independently monitored by one of the facility PLCs which proportionally opens or closes the BC's flow control valve to keep the level near the desired set point.

The BC level sensing port extends vertically upward through the CL cryostat lid, where it connects through a miniature Conflat flange and capillary tube to an Omega PX319 absolute pressure sensor that monitors the pressure, AP_BC, inside the BC. A separate connection from this sense port is connected to the high-pressure inlet of a Dwyer 605 Magnehelic differential pressure transmitter, whose low-pressure inlet is connected to the CL's GN2 exhaust line to the low voltage side of its electrical isolator, to monitor the differential pressure, DP_HEX, of the GN2 flow through the CL HEX. The pressure drop through the exhaust line, from the electrical isolator to the vacuum tee immediately above the subcooling vacuum pump, DP_EXH, is similarly monitored by a separate Dwyer 605 transmitter.

To maintain low-pressure drop through the GN2 exhaust line we used an insertion type, Sierra Instruments FastFlo 620S flow meter to monitor the mass flow rate of GN2, Q_GN2 (see Fig. 16), exiting the CL. To maintain calibration accuracy, care was taken to provide appropriate upstream and downstream straight pipe lengths to condition the flow passing the meter.

Fig. 17 shows the arrangement of voltage tap pairs and temperature sensors used to characterize the performance of the CLs. The electrical performance for the entire length of the CL was piecewise monitored. The voltage measurements were of two sorts, either to monitor the bulk average performance of a continuous section or to monitor the behavior of the electrical joints between sections.

The voltage tap pair, V_OVRALL, monitors the voltage drop along the entire GN2-cooled portion of the HEX. Rather than installing temperature sensors within the HEX's stainless-steel boundary, the HEX was subdivided into three equal lengths, with the upper two, V_HI, and V_MID monitored separately, to permit approximate estimation of the bulk average temperature distribution along the HEX, based on the known resistivity versus temperature characteristic for OFHC copper. The voltage drop along each REBCO petal was similarly monitored by six voltage tap pairs, V_HTS1 through V_HTS6. To distinguish between the resistance of the REBCO tape to copper end fittings at the upper and lower ends of the REBCO petals, one petal was also equipped with a half-height voltage tap pair, V_HTSL, spanning the lower half of the petal.

The voltage tap pair, V_HBC, monitored the joint between the HEX and the BC lid. The pair, V_BC1, monitored the joint between the BC lid and base, whereas V_BC2, monitored the joint between the BC base and one of the REBCO petals. The voltage tap pair, V_TRM, is the average of two redundant signals that monitor the joint between the lower end of a REBCO petal and the VIPER cable jumper at the base of the lead.

Temperature sensors were also placed at strategic locations along the CL to monitor its cooling characteristics. Not all of the installed sensors are included in Fig. 17. The wide range of operating temperatures inside the CL cryostat inspired the use of Lake Shore Cernox CX-1070 and CX-1080 sensors for measurements ranging from 20 K to 77 K, and PT-102 platinum resistive temperature detectors (RTDs) for measurements ranging from 77 K to ambient. The Cernox sensors were deemed accurate to within $+/-50$ mK, with the RTDs accurate to within $+/-1$ K. Temperatures at the lower, T_HTSL_C, and upper, T_HTSU_C, ends of the REBCO lead sections are the average of two redundant Cernox sensor measurements at each location. Temperatures on the outer surface of the BC wall were monitored using Cernox sensors mounted 80 mm (T_BCS_80), 120 mm (T_BCS_120), and 165 mm (T_BCS_165) above the BC's zero-liquid level, and by a platinum RTD mounted to the BC's stainless-steel cap, T_BC_SS. In the data reduction section, this RTD will be referred to at T_IN, on the assumption that the GN2 entering the HEX is nominally at the same temperature as its surrounding stainless-steel boundary.

The temperature of the GN2 exiting the upper end of the HEX, T_GN2_EXH, is the average reading from two, insertion-type Omega Instruments RTD-801 sensors installed within the exhaust plena to either side of the CL, whereas that measured at the base of the ambient temperature current terminal, T_TRMU, was monitored by a Lake Shore PT-102 sensor. Although the temperature of the terminal cooling water supplied to the ambient temperature current terminal was well regulated by the heater/chiller unit, its return temperature, T_CL_H2O, varied with the operating current and was measured separately by an insertion-type IFN TM4331 RTD.

VII. Measured and Predicted Performance

The CLs have run five times along with the test facility [9], [10]. Most data presented in this section comes from the fourth of those tests performed at MIT-PSFC during September 2022 as part of a research project with CFS. This CL performance assessment campaign was specifically arranged to verify the performance of the CLs relative to design expectations, in a standalone configuration where they were electrically connected at the end of the cold buses. The analysis tools outlined in Section III were used to directly compare predicted and measured performance across: temperature, voltage, exhaust gas temperature, exhaust mass flow, and pressure drop. The critical current of the REBCO section was not directly measured due to the risk of permanent damage so simulation was used to compare the operation to the critical surface.

The CLs were cooled down from room temperature in $\sim$18 h to minimize differential thermal stresses and match the cooling rate of the cryostat thermal shields. Filling to 80 mm LN2 level in the BCs took another $\sim$1 hr. The CLs ran for $\sim$8 weeks during the TFMC testing campaign, $\sim$4 weeks during the CL performance assessment campaign, and $\sim$7 weeks during subsequent projects. During the initial cooldown of the CLs, it was noticed that significant condensation and icing occurred at the stainless top flange of each CL due to poor humidity control in the test

hall. The heater/chiller was able to maintain a temperature of ~30 C at the top of the CLs, although the nitrogen exhaust was at or below the dew point depending on the transport current. A system of fans was installed to convectively warm the CLs and evaporate the moisture, and this worked successfully for all remaining tests.

Table III summarizes measured and simulated electrical resistances of various sections of the CLs at 120 mm LN2 level and the associated VIPER cable bus. All indium joints show very low resistance and the overall simulation matches measurement well.

Fig. 18 summarizes the temperature measurements at various locations along the CLs. All plots in this sequence show the measured temperature on the *y*-axis, the height of LN2 in the BCs on the *x*-axis, and a different trace for each operating current. Fig. 18(a) and (b) shows measured results at a nominal BC pressure of 1.02 bar-a, whereas Fig. 18(c) also includes results during subcooled operation of the CLs at 0.62 bar-a.

Fig. 18(a) shows the variation in the temperatures measured at the upper end of the REBCO lead sections versus LN2 level in the BCs at different operating currents when the boil-off GN2 is exhausted at atmospheric pressure. The measurements show a very slight decrease in temperature with increasing LN2 level and a slight increase in temperature with increasing current. Even so, all temperatures remain within about 1 K of the computed saturation boiling temperature, T_{sat}, for the BC LN2, based on the measured absolute pressure in the BC, *AP_BC*. That is, the LN2 in the BCs is fulfilling the first of its intended functions—to provide near-constant thermal intercept at the upper ends of the REBCO lead sections. Because the BC level control scheme uses a proportional controller, the fill level deviates slightly from its target value as the operating current varies.

Fig. 18(b) shows the variations in the temperatures measured by the CX-1080 Cernoxes mounted at the 80 mm, *T_80*, and 120 mm, *T_120,* elevations on the external sidewalls of the BC versus LN2 level at various operating currents. The vertical dashed lines in the figure were drawn by hand to help guide the eye and show the respective Cernox mounting locations. The data trace for each sensor in Fig. 18(b) show a clear breakpoint as the LN2 level passes the elevation of the sensor. This makes sense as LN2 heat transfer is significantly higher than that of GN2, resulting in a decreased slope and confirms that the LN2 level processing method is accurate. At the maximum LN2 level, the completely full BC wall temperatures approach to within a degree or so of the BCs' computed saturation boiling temperatures. At each elevation, the 3-D BC modeling indicates near-uniform temperature through the thickness of the BC wall. Hence, the variation in the measured BC wall temperatures were used to confirm the assumed boiling heat transfer coefficients applied to the BCs in the model [see Fig. 21(c)].

Fig. 18(c) shows the temperature variation versus LN2 level measured by the insertion-type Pt RTD installed in the GN2 exhaust at the outlet from the CL HEXs for both atmospheric boiling and subcooled operation. The readings show a slight decrease in temperature with increasing LN2 level, and roughly 5–10 K increase between each operating current level. There is perhaps a very slight decrease in temperature when the CL is

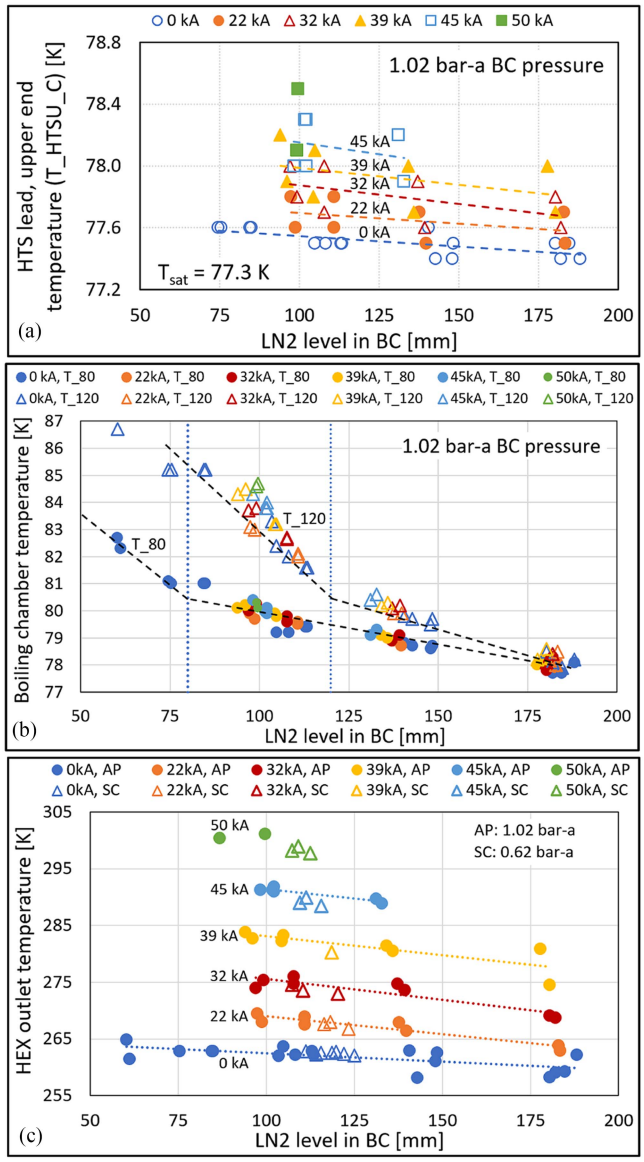

Fig. 18. Temperature versus BC LN2 levels at (a) upper ends of REBCO sections (T_ HTSU_C), (b) two elevations (T_ BCS_80 and T_ BCS_120) on the BC sidewalls, and (c) in the exhaust plena (T_ GN2_EXH) at the upper ends of the CLs at 0.62 bar-a and 1.02 bar-a pressures. Dashed lines represent linear regression fits meant to help guide the eye.

operated with reduced (0.62 bar-a) pressure in the BCs, although the trend is not all that significant.

During subcooled operation, the pressure in the BCs could be stably reduced to below roughly 0.65 bar-a. At zero current, the mass flow rate at pressures above that was low enough that the subcooling vacuum pump reached the lower limit of its variable frequency drive and could no longer run continuously. When operating at reduced pressure, the WEKA flow control valves have a reduced range of openings due to the higher differential pressure across the valve. This keeps the level in the BC more constant than at atmospheric boiling conditions. Trends during this reduced pressure operation matched very closely the trends of atmospheric operation, with temperatures at the upper end of the REBCO sections remaining within <1 K above the computed LN2 saturation temperature of 73.4 K.

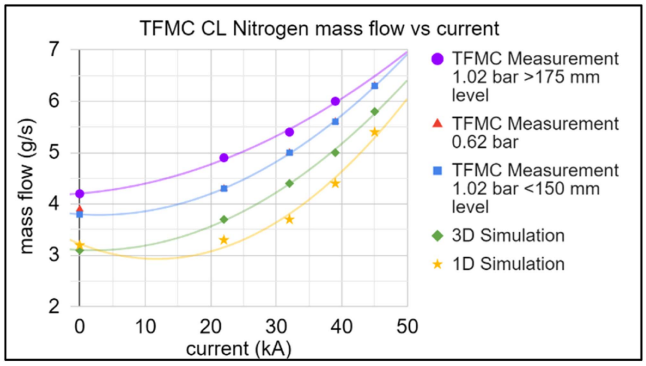

Fig. 19. Measured and predicted exhaust nitrogen mass flow versus power supply. The second-order polynomial fits are shown to help guide the eye.

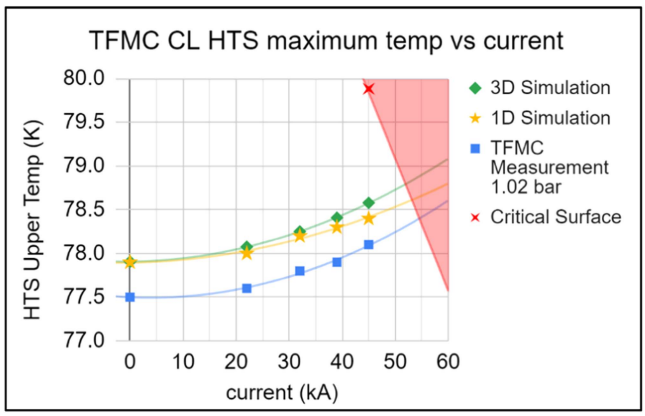

Fig. 20. Measured and simulated REBCO section upper temperature (T_HTSU_C) when operating at 1.02 atm and simulated critical surface. The second-order polynomial regression fits are shown to help guide the eye.

Fig. 19 shows nominally the same mass flow rate versus current for both atmospheric and 0.62 bar-a subcooled operation. This is reasonable as the same enthalpy flows into the BCs from the cryostat's LN2 reservoir, although the distribution of that enthalpy among liquid and gas differs for the two cases. The subcooling operation is in some ways easier for short-duration tests as it allows operation over a narrower range of reservoir levels and WEKA valve opening position. It can also be seen that when the level in the BC is raised significantly above 175 mm, it overflows the BC Lid and touches the base of the HEX. This results in significantly higher mass flow rates which can be attributed to a reduction in conduction length across the lid and sidewalls of the BCs. The simulated mass flow from the 3-D COMSOL code is roughly 0.5 g/s lower than the measured value at all operating currents. This can be partially attributed to thermal radiation heating the resistive portions of the CLs from the cryostat lid which were not included in the models.

Ideal nitrogen-gas-cooled binary CLs have a minimum heat inleak of between 23 and 30 W/kA [55], [56], [12], although these values are difficult to achieve in practice. Mass flow measurements indicate that the as-built CLs have minimum heat inleak of ~28 W/kA at 50 kA, indicating they are very close to this optimal value. Extraction of gaseous nitrogen at the base of the room temperature terminal and hard-to-quantify conduction heat leak via the PS connections add some uncertainty to these calculations.

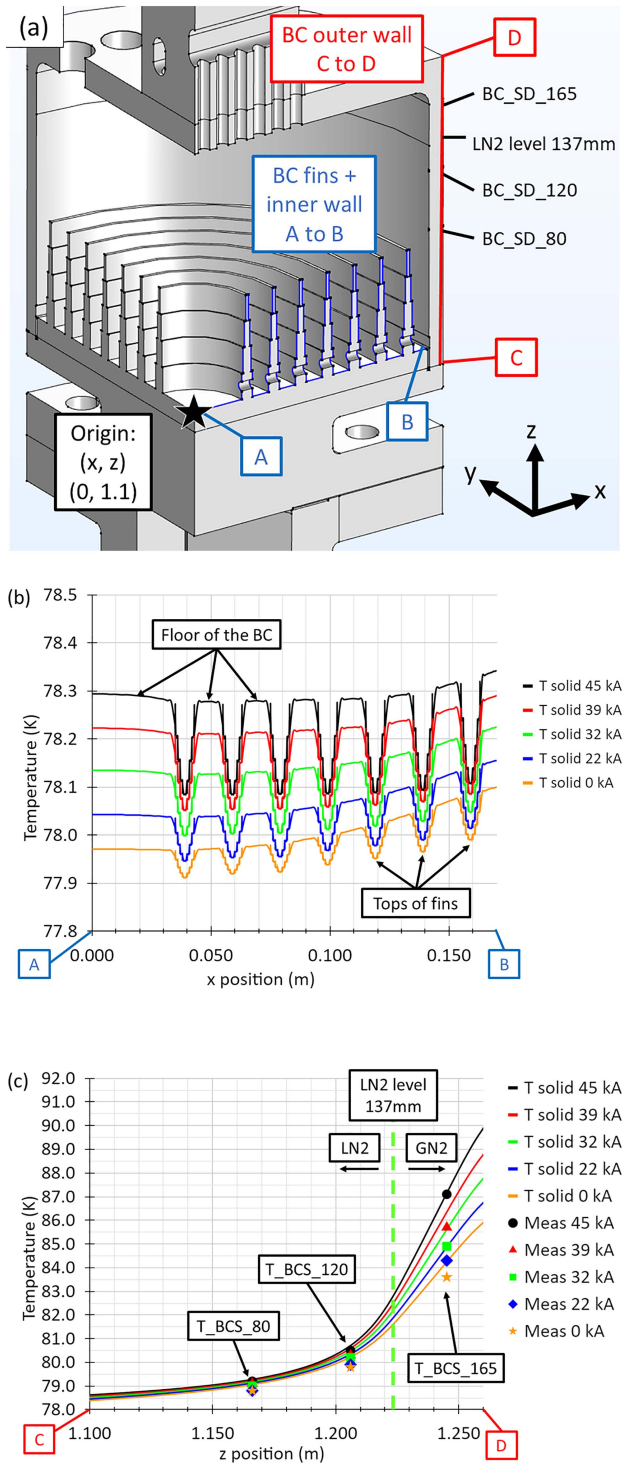

Fig. 21. (a) 3-D COMSOL model image showing the edges selected for plotting. (b) Temperature inside the BC along the fins from points A to B versus *X* position during atmospheric pressure LN2 boiling. (c) Temperature along the outer diameter of the BC wall between points C and D compared to measured values T_BCS_80, T_BCS_120, and T_BCS_165 versus the *z* position.

Fig. 20 shows that the measured REBCO section upper temperatures were ~0.5 K lower than the 3-D simulated values for atmospheric pressure boiling. This lends more conservatism to the REBCO section critical current predictions in Fig. 20 and

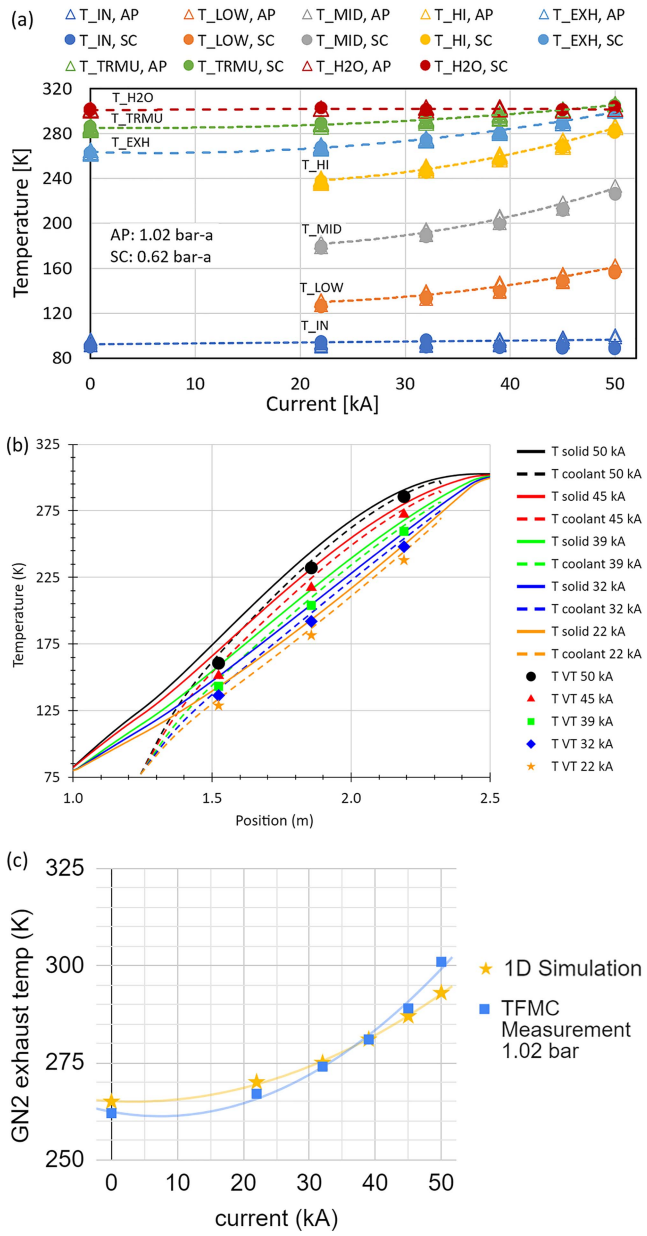

Fig. 22. (a) Measured temperatures along the CLs in atmospheric and reduced pressure boiling conditions. (b) Simulated temperatures from 1-D MATLAB model and HEX voltages converted to temperatures. (c) HEX measured and simulated temperatures from 3-D COMSOL model. (d) Simulated versus measured nitrogen exhaust temperatures (T_GN2_EXH) when operating at atmospheric pressure and 137 mm LN2 level. The second-order polynomial regression fits are shown to help guide the eye.

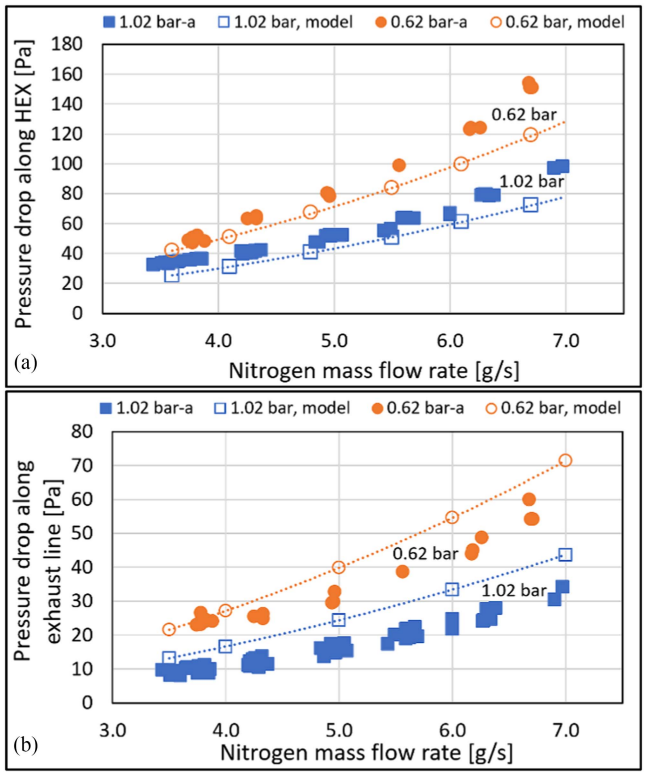

Fig. 23. Differential pressure versus mass flow rate across (a) HEX (DP_HEX). (b) Remaining GN2 exhaust lines (DP_EXH). Dashed second-order polynomial regression fits are shown to help guide the eye.

suggests the CLs could operate stably up to ~55 kA before thermally quenching.

Fig. 21 shows the temperatures of the BC fins and the outside wall of the BC as a function of current compared to the measured temperature values taken on the outside wall, T_BCS_80, T_BCS_120, and T_BCS_165. The results show that the LN2 boiling heat transfer equations used give very good agreement of temperatures to the measured values.

Fig. 22(a) demonstrates that measured temperatures along the HEX portion of the CLs are minimally affected by pressure and temperature changes within the BC. For this plot, the computed bulk average resistivity for each HEX section, *Ri(Ti, I)*, where *i* denotes the HEX section label, was used to compute the section's bulk average temperature, *Ti*, for each operating current, *I*. The *T_LOW*, readings were created by subtracting the *V_HI* and *V_MID* voltages from the *V_OVRALL* measurement when computing the section resistances. These same temperatures, plotted over top of the 1-D MATLAB temperature outputs in Fig. 22(b), show good agreement.

Variations in HEX's GN2 exhaust temperature as a function of current at 1.02 bar BC pressure are accurately predicted in the 1-D MATLAB code as shown in Fig. 22(c). This gives high confidence in the overall energy balance of the simulations.

As the mass flow through the CLs increases, so too does the pressure drop across the HEX. This increases the pressure of LN2 boiling within the BC which in turn increases the boiling temperature of the liquid (a 1000 Pa pressure increase raises the boiling temperature by roughly 0.1 K). Critical current margins are highly affected by these temperature changes as shown in Fig. 20 and thus the pressure drop across the HEX should be minimized as much as possible. The measured values are shown in Fig. 23. Simulated values of flow through the HEX are from a 3-D COMSOL model, and those through the exhaust lines are from 1-D pipe pressure drop calculators. The HEX simulations are relatively simple to set up and run when compared to those required for the 'meandering flow' type heat exchangers within the ITER CLs [18]. The design of the HEX results in very low-pressure drop due to the many straight channels arranged in parallel which have sufficient cross-sectional area.

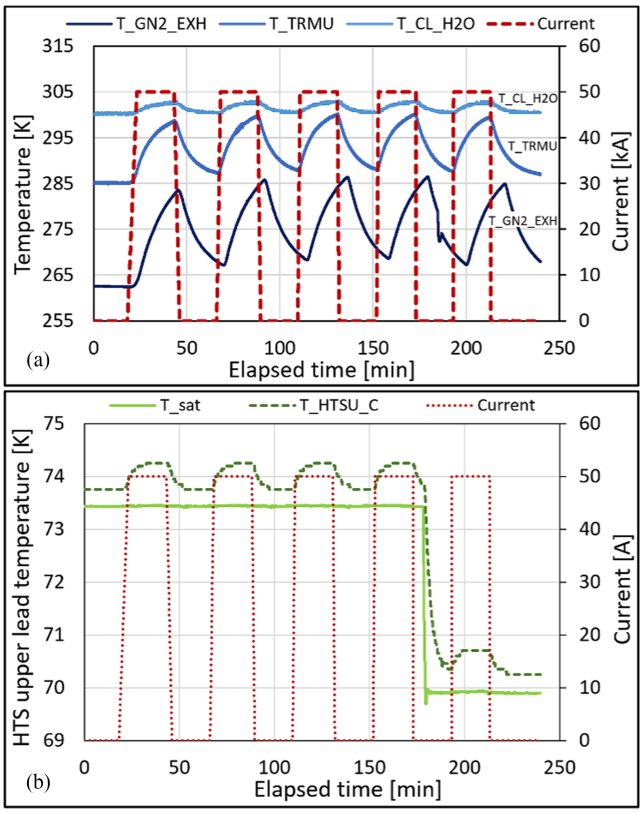

Fig. 24. CL response to progressively increasing current ramp rates up to 17 kA/s up-ramp and 50 kA/s down-ramp current profiles. (a) Temperatures at the CL HEX (left axis) and PS current (right axis) versus elapsed time. (b) HTS section temperatures and PS current versus elapsed time with BC saturation temperatures. The first four ramps occur at 0.62 bar and the final ramp is at 0.38 bar.

As a precursor to the CLs now being designed for operation in SPARC by CFS, another goal of the research project was to confirm that no extraneous heat was generated under fast ramping conditions that could result in thermal runaway. Fig. 24 shows the response of the CLs from idle to 50 kA with progressively increasing current up-ramps as high as 17 kA/s and down-ramps as high as 50 kA/s while operating at a reduced pressure of 0.62 bar. Overall the reaction to high ramp rates is minimal with temperatures in the HEX stabilizing within ∼10 min and temperatures in the REBCO section settling within ∼20 min.

Knowing that the last, fastest-ramped current profile in Fig. 24 was the to be the final element in the CL performance assessment campaign, we decided to use that opportunity to extend the operating range of the BC subcooling vacuum pumps downward. The rapid drop in the T_sat reading to 69.9 K at roughly 180 min elapsed time in Fig. 24(b) corresponds to a reduction in the BC pressure from 0.62 bar to 0.38 bar. The BC pressure during this step undershot slightly but stabilized within roughly 4 min duration. The temperatures measured near the upper ends of the HTS leads lagged slightly behind, approaching within ∼1 K of T_sat within about 13 min.

VIII. Conclusion

This article presents the novel design and operation of optimized LN2-cooled REBCO CLs used to power the SPARC TFMC and capable of transferring 50 kA steady-state current and 50 kA/s fast ramping to a <20 K test article while having ∼5 W of thermal conduction heat leak per CL. The short two-year schedule requirement for the design and build of the CLs drove multiple innovations in the design including the use of optimization for LN2 cooling, demountable indium wire seals, and a parallel-segmented REBCO section. The testing also confirmed that subatmospheric pressure LN2 cooling is reliable and can provide additional temperature margin at the warm end of the REBCO section.

This design represents a significant step forward in CL design and enables high-performance CL builds on tight schedules and without the need for significant helium cryogenic facilities. These CLs are enabling MIT to test a variety of high-power R&D magnets and will become integral in the design and operation of the SPARC tokamak being built by CFS.

Acknowledgment

The parties have pursued patent protection relating to inventions. CFS has exclusive commercial rights to the technology for energy generation. The magnet technology in the TFMC Program was developed under research collaborations between MIT and Commonwealth Fusion Systems.

References

[1] Z. Hartwig et al., "The SPARC toroidal field model coil program," *IEEE Trans. Appl. Supercond.*, vol. 34, no. 2, Mar. 2024, Art. no. 0600316.
[2] Z. Hartwig et al., "VIPER: An industrially scalable high-current high-temperature superconductor cable," *Supercond. Sci. Technol.*, vol. 33, 2020, Art. no. 11LT01.
[3] E. Salazar et al., "Fiber optic quench detection for large-scale HTS magnets demonstrated on VIPER cable during high-fidelity testing at the SULTAN facility," *Supercond. Sci. Technol.*, vol. 34, no. 3, 2021, Art. no. 035027.
[4] V. Fry, J. Estrada, P. Michael, E. Salazar, R. Vieira, and Z. Hartwig, "Simultaneous transverse loading and axial strain for REBCO cable tests in the SULTAN facility," *Supercond. Sci. Technol.*, vol. 35, no. 7, 2022, Art. no. 075007.
[5] B. LaBombard et al., "Grooved, stacked-plate superconducting magnets and electrically conductive terminal blocks and related construction techniques," U.S. Patent US11417464, Aug. 16, 2022.
[6] D. Whyte, "Small, modular and economically attractive fusion enabled by high temperature superconductors," *Philos. Trans. Roy. Soc. A*, vol. 377, 2019, Art. no. 20180354, doi: 10.1098/rsta.2018.0354.
[7] A. Creely et al., "Overview of the SPARC tokamak," *J. Plasma Phys.*, vol. 86, no. 5, 2020, Art. no. 865860502.
[8] R. Vieira et al., "Design, fabrication, and assembly of the SPARC Toroidal Field Model Coil," *IEEE Trans. Appl. Supercond.*, early access, Jan. 22, 2024, doi: 10.1109/TASC.2024.3356571.
[9] T. Golfinopoulos et al., "The SPARC toroidal field model coil test facility," submitted for publication.
[10] P. C. Michael et al., "A 20-K, 600-W, cryocooler-based, supercritical helium circulation system for the SPARC Toroidal Field Model Coil Program," *IEEE Trans. Appl. Supercond.*, vol. 34, no. 2, Mar. 2024, Art. no. 0600113.
[11] D. G. Whyte et al., "Experimental assessment and model validation of the SPARC Toroidal Field Model Coil," *IEEE Trans. Appl. Supercond.*, vol. 34, no. 2, Mar. 2024, Art. no. 0600218.
[12] P. Herrmann et al., "Cryogenic load calculation of high Tc current lead," *Cryogenics*, vol. 33, no. 5, pp. 555–562, 1993.
[13] M. Wilson, *Superconducting Magnets*. New York, NY, USA: Oxford Univ. Press, 1989, pp. 266–267.
[14] Y. Iwasa, *Case Studies in Superconducting Magnets*. New York, NY, USA: Plenum, 2002, pp. 125–134.
[15] A. Zhukovsky, "TFMC cooling by LHe; CL cooling with gas He and LN2," Internal Memo, Aug. 8, 2019.
[16] A. Zhukovsky, "Conceptual design 50 kA current lead resistive parts for TFMC with LN2 cooling," Internal Memo, Nov. 24, 2019.

[17] R. L. Boivin and C. T. Reddy, "Cryogenic system for the alcator C-mod tokamak," in *Proc. 15th IEEE/NPSS Symp. Fusion Eng.*, 1993, vol. 1, pp. 333–336.

[18] P. Bauer et al., "Development of HTS current leads for the ITER project," *IOP Conf. Ser., Mater. Sci. Eng.*, vol. 756, 2020, Art. no. 012032.

[19] R. Heller et al., "Experimental results of a 70 kA high temperature superconductor current lead demonstrator for the ITER magnet system," *IEEE Trans. Appl. Supercond.*, vol. 15, no. 2, pp. 1496–1499, Jun. 2005.

[20] W. Fietz, R. Heller, A. Kienzler, and R. Lietzow, "Status of HTS current leads for WENDELSTEIN 7-X and JT-60SA," *Fusion Eng. Des.*, vol. 84, no. 2–6, pp. 776–779, 2009.

[21] W.-B. Xi et al., "Study on the operation safety of HTS current leads in EAST device," *J. Fusion Energy*, vol. 34, pp. 111–115, 2014.

[22] R. Heller et al., "70 kA high temperature superconductor current lead operation at 80 K," *IEEE Trans. Appl. Supercond.*, vol. 16, no. 2, pp. 823–826, Jun. 2006.

[23] R. McFee, "Optimum input leads for cryogenic apparatus," *Rev. Sci. Instrum.*, vol. 30, pp. 98–102, 1959.

[24] P. F. Herrmann, "Section D10. Current leads," in *Handbook of Applied Superconductivity*. Philadelphia, PA, USA: Institute of Physics Publishing, 1998.

[25] W. Bing, P. Quan-Ling, Y. Xiang-Chen, and L. Shao-Peng, "Current leads for superconducting magnets of ADS injector I," *Chin. Phys. C*, vol. 38, no. 6, 2014, Art. no. 067004.

[26] H. Brueck et al., "Results of the magnetic measurements of the superconducting magnets for the European XFEL," *IEEE Trans. Appl. Supercond.*, vol. 26, no. 4, Jun. 2016, Art. no. 4902204.

[27] R. Heller et al., "Development of forced flow cooled current leads for fusion magnets," *Cryogenics*, vol. 41, no. 3, pp. 201–211, 2001.

[28] A. Ballarino, "Current leads for the LHC magnet system," *IEEE Trans. Appl. Supercond.*, vol. 12, no. 1, pp. 1275–1280, Mar. 2002.

[29] Y. Park et al., "Design, fabrication and commissioning of the KSTAR TF current feeder system," *Fusion Eng. Des.*, vol. 86, no. 6–8, pp. 1440–1444, 2011.

[30] G. Citver, "Thermal tests of 6 KA HTS current leads for the tevatron," in *Proc. Cryogenic Eng. Conf.*, 1999, pp. 1549–1556.

[31] Y. Bi et al., "Development of 12 kA HTS current lead for accelerator magnet test application," *IEEE Trans. Appl. Supercond.*, vol. 23, no. 3, Jun. 2013, Art. no. 4800404.

[32] Y. Bi et al., "Development of 16 kA HTS current leads for 40 T hybrid magnet application," *J. Phys., Conf. Ser.*, vol. 507, 2014, Art. no. 032013.

[33] H. Bai, W. Marshall, M. Bird, A. Gavrilin, and H. Weijers, "Current leads cooling for the series-connected hybrid magnets," *AIP Conf. Proc.*, vol. 1573, pp. 1707–1712, 2014.

[34] W. S. Marshall et al., "HTS current leads for the NHMFL series-connected hybrid magnet," *IEEE Trans. Appl. Supercond.*, vol. 23, no. 3, Jun. 2013, Art. no. 4800905.

[35] J. R. Miller, G. E. Miller, S. J. Kenney, D. E. Richardson, and C. L. Windham, "Design and development of a pair of 10 kA HTS current leads for the NHMFL 45 hybrid magnet system," *IEEE Trans. Appl. Supercond.*, vol. 15, no. 2, pp. 1492–1495, Jun. 2005.

[36] W. Marshall et al., "Design of Nw cooled Bi-2223 HTS current leads for use in 0.4T field for the NHMFL series connected hybrid magnet," *AIP Conf. Proc.*, vol. 1573, pp. 1018–1025, 2014.

[37] A. Molodyk et al., "Development and large volume production of extremely high current density YBa2Cu3O7 superconducting wires for fusion," *Sci. Rep.*, vol. 11, 2021, Art. no. 2084.

[38] N. Strickland et al., "Extended-performance 'supercurrent' cryogen-free transport critical-current measurement system," *IEEE Trans. Appl. Supercond.*, vol. 31, no. 5, Aug. 2021, Art. no. 9000305.

[39] R. Shutt, M. Rehak, and K. Hornik, "Gas cooled leads," Brookhaven National Laboratory, Associated Universities, Inc., Long Island, NY, USA, 1993.

[40] R. Heller, "Numerical calculation of current leads for fusion magnets," Institut fur Technische Physik, Kernforschungszentrum Karlsruhe GmbH, Karlsruhe, Germany, 1989.

[41] R. Shutt, M. Rehak, and K. Hornik, *Gas Cooled Leads. Part 1, Theoretical Study*. Upton, NY, USA: Brookhaven National Lab, 1993.

[42] W. Frost, *Heat Transfer at Low Temperatures*. New York, NY, USA: Springer, 1975.

[43] E. Brentari, P. Giarratano, and R. Smith, *Boiling Heat Transfer for Oxygen, Nitrogen, Hydrogen, and Helium*, vol. 317. Boulder, CO, USA: U.S. National Bureau of Standards, 1965.

[44] J. Seader, W. Miller, and L. Kalvinskas, *Boiling Heat Transfer for Cryogenics*. Washington, DC, USA: National Aeronautics and Space Administration, 1965.

[45] V. Gregoriev, Y. Pavlov, and U. Amestistov, *Boiling of Cryogenic Liquids*. Moscow, Russia: Energiya, 1977.

[46] B. A. Smith et al., "A pulsed magnetic field test facility for conductors and joints," *IEEE Trans. Appl. Supercond.*, vol. 32, no. 4, pp. 2292–2295, Jul. 1996.

[47] A. E. Haight, M. M. Haynes, L. A. Bromberg, M. Takayasu, P. C. Michael, and A. Radovinsky, "Re-makeable joint with insulation for REBCO superconductor cables," *IEEE Trans. Appl. Supercond.*, vol. 29, no. 5, Aug. 2019, Art. no. 4802105.

[48] F. Mangiarotti, "Design of demountable toroidal field coils with REBCO superconductors for a fusion reactor," Ph.D. dissertation, Dept. Nuclear Sci. Eng., MIT, Cambridge, MA, USA, 2016.

[49] Y. Takahashi et al., "Development of ITER-CS model coil terminal assembling by using indium wires," *Fusion Eng. Des.*, vol. 58/59, pp. 93–97, 2001.

[50] D. Fraser, "Special indium seal for cryogenic use," *Rev. Sci. Instrum.*, vol. 33, pp. 762–763, 1962.

[51] C. Lim, "Indium seals for low-temperature and moderate-pressure applications," *Rev. Sci. Instrum.*, vol. 57, pp. 108–114, 1986.

[52] R. Turkington and R. Harris-Lowe, "Note on the design of simple indium O-ring seals," *Rev. Sci. Instrum.*, vol. 55, pp. 803–805, 1984.

[53] S. Döge and J. Hinger, "A hydrogen leak-tight, transparent cryogenic sample container for ultracold-neutron transmission measurements," *Rev. Sci. Instrum.*, vol. 89, 2018, Art. no. 033903.

[54] B. Zhang, H. Hong, and M. Yu, "Leakage analysis and ground tests of knife edge indium seal to lunar sample return devices," *Proc. Inst. Mech. Eng., Part G: J. Aerosp. Eng.*, vol. 233, no. 6, pp. 2010–2022, 2018.

[55] A. Ballarino, "Current leads, links and buses," in *Proc. CAS-CERN Accel. School, Supercond. Accel.*, 2013, pp. 547–558.

[56] P. Herrmann et al., "Test results of a 1 kA (2 kA)–20 kV HTSC current lead model," *Cryogenics*, vol. 34, no. 6, pp. 543–548, 1993.